Aalto University

School of Electrical Engineering

Degree Programme of Communications Engineering

Christos Karaiskos

Altruistic Transmit Beamforming for Cross-layer Interference Mitigation in Heterogeneous Networks

Master's Thesis

Espoo, December 14, 2012

Supervisor: Professor Jyri Hämäläinen
Instructor: Dr. Alexis Dowhuszko

Aalto University

School of Electrical Engineering

Degree Programme of Communications Engineering

ABSTRACT OF
MASTER'S THESIS

Author:	Christos Karaiskos
Title:	
Altruistic Transmit Beamforming for Cross-layer Interference Mitigation in Heterogeneous Networks	

Date:	December 14, 2012	**Pages:**	10 + 86
Major:	Radio Communications	**Code:**	S-72
Supervisor:	Professor Jyri Hämäläinen		
Instructor:	Dr. Alexis Dowhuszko		

The emergence of heterogeneous networks, with low-power nodes operating under the umbrella of high-power macro cells, simplifies planning procedures for operators, but introduces the problem of cross-layer interference between the overlapping cells. An effective technique for combating interference is transmit beamforming (TBF), a transmitter-side technique which utilizes partial knowledge of the channel and presence of multiple antennas at the transmitter to enhance the signal reception quality at a receiver. When applied to the base station associated with the receiver, TBF boosts the desired signal. On the other hand, when applied to the interfering base station, TBF reduces the effect of the interference signal. The former technique is commonly referred to as egoistic TBF, while the latter is known as altruistic TBF. In this thesis, we provide theoretical evaluation of the performance gains that altruistic TBF is able to offer to a heavily interfered user in a heterogeneous setting, when channel state information is conveyed from the receiver to the transmitter through a limited feedback channel. We show that the application of altruistic TBF to specifically defined clusters of interferers is able to drastically improve performance for the victim user. Furthermore, we prove the exact upper bound for the performance of the victim user, when only phase feedback is used for altruistic TBF and the source of interference is a single dominant interferer. Finally, we investigate and propose new techniques that can be applied to multi-antenna heterogeneous network scenarios for interference mitigation purposes.

Keywords:	heterogeneous networks, femtocells, interference mitigation, MIMO, closed-loop methods, transmit beamforming, cross-layer interference
Language:	English

Acknowledgements

Espoo, December 14, 2012

Christos Karaiskos

List of Abbreviations

3G	3rd Generation
BS	Base Station
BU	Base Unit
CAPEX	CAPital EXpenditure
CDF	Cumulative Distribution Function
CL	Closed Loop
CLT	Central Limit Theorem
CoMP	Coordinated Multi-Point
CS/CB	Cooperative Scheduling/Beamforming
CSG	Closed Subscriber Group
CSIT	Channel State Information at the Transmitter
CU	Central Unit
DCS	Dynamic Cell Selection
DoA	Direction of Arrival
DTD	Delay Transmit Diversity
EGT	Equal Gain Transmission
FBS	Femto Base Station
FDD	Frequency Division Duplex

FFR	Fractional Frequency Reuse
FUE	Femto User Equipment
GPS	Global Positioning System
HetNet	Heterogeneous Network
i.i.d.	Independent and Identically Distributed
JP	Joint Processing
JT	Joint Transmission
LTE	Long Term Evolution
MBS	Macro Base Station
MISO	Multiple Input Single Output
MUE	Macro User Equipment
OL	Open Loop
OPEX	OPerational EXpenditure
OTD	Orthogonal Transmit Diversity
PBS	Pico Base Station
PC	Power Control
PDF	Probability Density Function
PPC	Partial Phase Combining
PSTD	Phase Sweep Transmit Diversity
QoS	Quality of Service
RF	Radio Frequency
RN	Relay Node
RRH	Remote Radio Head

RV	Random Variable
RVQ	Random Vector Quantization
SDT	Selection Diversity Transmission
SIC	Successive Interference Cancellation
SINR	Signal-to-Interference plus Noise Ratio
SNR	Signal-to-Noise Ratio
STS	Space Time Spreading
STTD	Space Time Transmit Diversity
TAS	Transmit Antenna Selection
TBF	Transmit Beamforming
TDD	Time Division Duplex
TSC	Transmitter Selection Combining
TSTD	Time Switched Transmit Diversity
TTI	Transmission Time Interval
UE	User Equipment
VQ	Vector Quantization
WCDMA	Wideband Code Division Multiple Access

Contents

Chapter 1

Introduction

The appearance of high-performance terminals in the market has triggered the burst of novel services and applications that require ubiquitous internet connectivity and enhanced data rates (see Fig. 1.1). To deal with this unprecedented change in capacity demands, mobile operators are in the process of expanding their traditional macro cell network deployments with supplemental infrastructure.
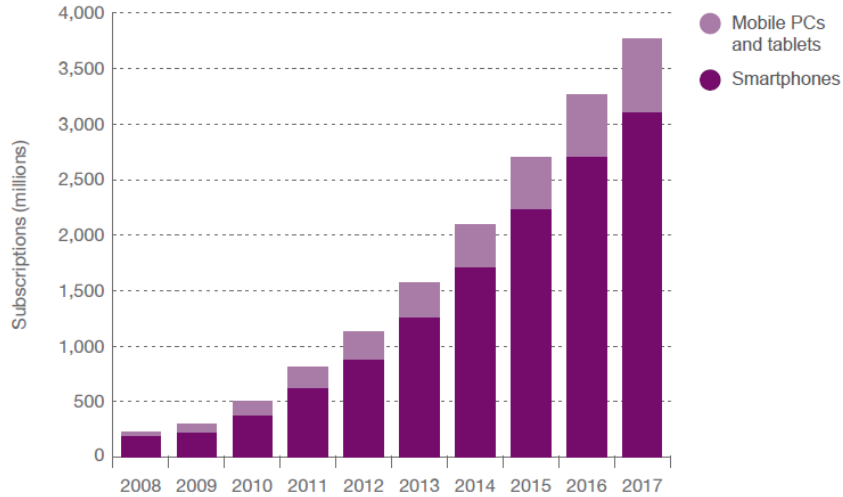
Figure 1.1: The number of mobile subscriptions involving smartphones, tablets and PCs is expected to retain its exponential growth in the following years, exceeding 3 billion subscriptions by 2017 [1].
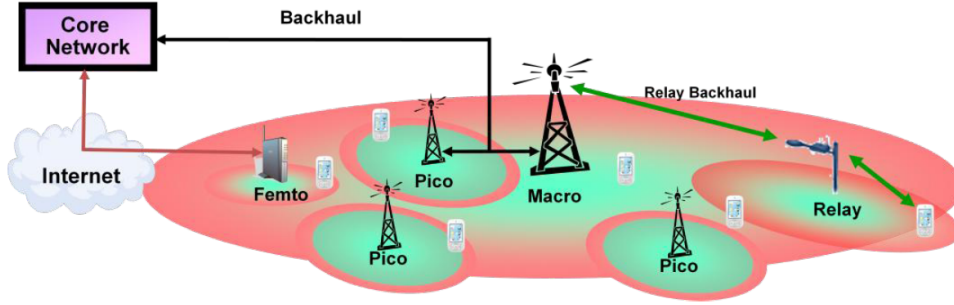
Figure 1.2: Illustration of a heterogeneous network, including overlaid deployments of macro, pico, relay and femto nodes [2].

Techniques involving traditional macro cell-splitting have been abandoned, not only because of the already high density of macro cells in the geographical landscape, but also due to the high capital expenditure (CAPEX) and operational expenditure (OPEX) associated with each installation [3]. Instead, a turn towards overlaid cell deployments (see Fig. 1.2) consisting of a mixture of macro nodes, remote radio heads and low-power pico, femto and relay nodes is promoted [4]. In contrast to macro base stations, the newly-introduced nodes have the advantage of low transmit power, small physical size, low cost and less demanding planning procedures.

The elements of a heterogeneous network deployment can be briefly classified in:

- *Macro Base Stations* (MBSs) provide wide area coverage and act as an umbrella cell for all other layers. Typically, their transmission power can reach 46 dBm.

- *Remote Radio Heads* (RRHs) are small-sized, easily mountable units which perform basic radio-frequency (RF) operations and forward signals to a Base Unit (BU) for baseband processing. The back-haul link connecting RRHs with their BU is usually optical fiber, to avoid extensive round-trip latency.

- *Pico Base Stations* (PBSs) resemble macro base stations but require lower transmit power. The 3GPP specifications define pico TX power to be 20-24 dBm, but for some manufacturers 'pico' products may have power up to 33dBm.

- *Relay Nodes* (RNs) extend the wireless link between cell-edge users and their serving MBS by acting as a pipeline [5].

- *Femto Base Stations* (FBSs) are plug-and-play indoor base stations (BSs) that typically transmit with lower powers than 20 dBm [6]. Unlike all the previously mentioned nodes, femto nodes are owned and installed individually by end users, therefore their exact placement cannot be planned by the operator.

The presence of heterogeneous elements in the network provides flexibility in site acquisition and lower total expenses for the operator, while it also promotes seamless broadband experience for subscribers. Furthermore, from an environmental point of view, it decreases unnecessary energy consumption. The most important feature of a heterogeneous network (HetNet), though, is the capability of simultaneous transmission over the same frequency bands, resulting in better utilization of the limited spectrum resources available to the operator.

1.1 Motivation

A major concern for the success of HetNets is the handling of *co-layer* and *cross-layer* interference. Co-layer interference is caused between nodes of the same type, while cross-layer interference involves nodes which belong to different tiers [6]. Usually, focus is given on cross-layer interference management scenarios involving macro and femto layers [7], due to the large power disparities between the two layers, the opportunistic user-deployed nature of the FBSs and, most importantly, the expected *closed subscriber group* (CSG) configuration for FBSs, which results to dead coverage zones both in downlink and uplink. In the downlink, CSG configuration forbids handover possibilities for a highly interfered *macro user equipment* (MUE) which is in the vicinity of an FBS. Conversely, in the uplink, the MUE is the source of interference and the victim is the nearby FBS, which cannot easily separate the incoming signal from its associated *femto user equipment* (FUE) from the interference. The work pursued in this thesis is motivated by the above observations and aims to provide effective and efficient solutions for dealing with the challenges of cross-layer interference.

1.2 Problem Context

Contemporary transmitters are equipped with multiple transmit antennas that can be utilized to provide additional degrees of freedom for the transmission of data. *Transmit beamforming* (TBF) [8] is a transmitter-side technique which utilizes multiple antennas to enhance the reception quality of a single symbol at a receiver equipped with a single receive antenna. In particular, TBF manipulates the signals of all transmit antennas in such a way that coherent combining is automatically performed at the target receiver. For TBF to work, it is vital that channel state information is available at the transmitter (CSIT). In frequency division duplex (FDD) systems, this can only be achieved through explicit feedback from the receiver, due to lack of reciprocity between downlink and uplink channel responses. Typically, TBF is used in an *egoistic* manner, aiming to shape signals of different antennas in such a way that they combine constructively at the receiver. This pre-adjustment provides a so-called beamforming gain at the receiver, since phases of the received signals are no longer random. Another use of TBF is to mitigate the channel strength between an interferer and a victim user who suffers from the emitted interference. In that case, TBF shifts its operation mode from egoistic to *altruistic*, aiming to shape the signals at the different antennas in such a way that they combine destructively at the victim user. This change of behavior from the interfering transmitter reduces interference at the victim user, but simultaneously sacrifices the beamforming gain previously observed at the served user.

Altruistic beamforming is an interference mitigation technique that could perfectly fit in the context of cross-layer downlink interference in two-tier macro-femto networks. Usually, in two-tier systems, the macro cell is modeled as primary infrastructure, since it promises ubiquitous coverage and is responsible for serving a larger number of subscribers [9]. For this reason, higher priority is commonly given to downlink interference scenarios, where the MUE is the victim. Indeed, consider the case where an MUE is in the vicinity of one or more co-channel CSG femto cells that operate simultaneously. Immediately, the signal-to-interference plus noise ratio (SINR) perceived by the MUE drops significantly, due to the strong incoming FBS interference and the weakened signal from its own MBS. On the other hand, it is typical that FUE operation benefits from the slowly varying indoor environment, the small distance between FBS and FUE and the presence of walls which act as a shield against outdoor signals. Thus, it

can be assumed that each FUE experiences very good quality of service (QoS) from its serving FBS, while the MUE is in a very disadvantageous position. Due to the very good channel conditions of the femto networks, it is possible that one or more FBSs act as donors by sacrificing the beamforming gain of their own users, in order to minimize the interference towards the MUE. The corresponding FUEs will not experience significant degradation of their SINR when losing their beamforming gain. This type of implicit cooperation from the interferer side can be transparent to the MBS, which continues its egoistic behavior.

1.3 Contribution

The purpose of this thesis is to utilize altruistic beamforming in cross-layer interference scenarios and derive theoretical and practical conclusions about its performance. More specifically, UTRA-based TBF algorithms, namely transmitter selection combining (TSC), g-mode 1 and g-mode 2, are modified to also serve as altruistic algorithms and are, then, applied to mitigate interference. For egoistic TBF, the algorithm of TSC is based on transmitting only through the strongest transmit antenna. The algorithm of g-mode 1 relies on equal gain transmission (EGT) and performs only phase adjustments among the transmit antennas, so that signals are combined constructively at the receiver. As an extension to g-mode 1, g-mode 2 ranks the amplitudes of the channel gains and allocates more power to the antennas corresponding to higher amplitude values. For altruistic TBF, the algorithm of TSC chooses the weakest transmit antenna, g-mode 1 performs only phase adjustments so that signals are combined destructively at the receiver, and g-mode 2 allocates more power to the weakest antennas in addition to phase adjustments. In summary, the goals of this thesis are to investigate the following topics:

1. In a single-macro, single-femto system where transmitters are equipped with 2 transmit antennas: Derive an exact upper bound for the receiver outage probability when the MBS applies egoistic beamforming using g-mode 1 with infinite number of feedback bits, and the FBS altruistic beamforming using g-mode 1 with infinite number of feedback bits. Algorithm g-mode 1 with infinite number of feedback bits is identical to EGT with perfect phase alignment.

2. In a single-macro, multiple-femto system where transmitters are equipped

with 2 transmit antennas: Derive the receiver outage probability when MBS applies egoistic beamforming using g-mode 1, g-mode 2 and the FBSs altruistic beamforming using g-mode 1, g-mode 2, when chi-squared approximations for the received signal powers are considered[1].

3. The signal-to-noise ratio (SNR) gain of a modified g-mode 2 algorithm for 2-antenna transmitters, in which soft information is utilized about the power difference between the two channel gains.

4. Schemes for interference mitigation for the case of 4 transmit antennas, by grouping antennas in pairs and using TSC, g-mode 1 and g-mode 2 for interference mitigation.

1.4   Thesis Organization

The thesis is organized in a total of 8 chapters. In chapter 2, the background needed for understanding the concept of egoistic transmit beamforming is provided and the specific transmit beamforming algorithms that will be used in this work are presented. Chapter 3 provides a literature review of commonly used interference management schemes for two-tier HetNets. Furthermore, the concept of altruistic beamforming is thoroughly explained and the egoistic TBF algorithms presented in chapter 2 are modified to handle interference mitigation.

Chapter 4 presents the generalized two-tier system model that will be used in the following two chapters. In particular, the scenario involves an indoor MUE which receives high interference from a group of surrounding CSG FBSs. Chapter 5 investigates the performance of perfect phase TBF (i.e. g-mode 1 with infinite number of bits for feedback message), in the presence of one dominant interferer FBS which is equipped with two transmit antennas. The MBS applies perfect phase egoistic TBF, while the dominant FBS applies perfect phase altruistic TBF. An exact closed-form expression is derived for the probabilistic behavior of the SINR at the interfered MUE.

Chapter 6 considers the performance improvements of the received SINR at the MUE when multiple two-antenna interferers perform altruistic TBF. The ideal number of altruistic interferers is investigated, for the particular system model

---

[1]Novel results of this part have been submitted for publication to the IEEE International Conference on Communications 2013 [10].

and scenario. In chapter 7, schemes that expand the performance of altruistic TBF algorithms are investigated. Finally, in chapter 8, conclusions are presented and possible future research directions to extend this work are also suggested.

Chapter 2

The Concept of Transmit Beamforming

Multiple antennas at the receiver can coherently combine the received signal paths so that the effects of the fading channel are alleviated, without the need for increased transmit power or bandwidth. Multiple antennas at the transmitter can also be exploited to enhance the received SNR of the served user, particularly in the downlink direction. Improvements in performance can be high, especially when using feedback schemes to provide the transmitter with knowledge of the channel response. With that knowledge, the transmitter can apply precoding techniques to shape its transmit symbols so that the instantaneous effect of the channel is mitigated. In this thesis, we will consider the multiple input single output (MISO) model; therefore, instead of 'precoding', the term 'transmit beamforming' will be used. The difference is that precoding is linked with MIMO systems and involves sending multiple data streams spatially through independent eigen-channels, while transmit beamforming implies single-layer transmission [8].

2.1 Classification of Transmit Diversity Methods

Transmit diversity utilizes the presence of multiple antennas at the transmitter in order to enhance the quality of the signal at the receiver side. Transmit diversity schemes have been mostly attractive for the downlink direction, since complexity issues (e.g. cost, power, space, processing) can be more easily managed at the BS

side. In general, transmit diversity modes are classified as open-loop (OL) and closed-loop (CL). This categorization stems from the fact that the former do not require the presence of CSIT, while the latter cannot function without it.

2.1.1 Channel State Information at the Transmitter Side

Unlike the receiver, the transmitter does not always have direct access to channel fading information. In principle, there are two possible methods of acquiring CSIT; in time division duplex (TDD) systems, CSIT can be obtained directly from estimation of the uplink channel (open-loop channel acquisition), while in FDD systems, the receiver is responsible for sending back information about the channel, due to lack of reciprocity between downlink and uplink (closed-loop channel acquisition) [11]. Presence of CSIT is considered critical for maximizing the achievable rates for users of the system. Despite its advantages, assuming complete CSIT is unrealistic, due to the uncertainty of the wireless medium and complications in CSIT acquisition.

2.1.2 Open-Loop Methods

In OL systems, the transmitter does not require knowledge of the channel. Therefore, such techniques do not depend on control information fed back by the receiver. In general, OL methods are favored against CL ones in situations involving high mobility or limitations in feedback capability. Different OL methods for multi-antenna systems have been proposed through the years, among which are Delay Transmit Diversity (DTD) [12], Orthogonal Transmit Diversity (OTD) [13], Space Time Spreading (STS) [14], Phase Sweep Transmit Diversity (PSTD) [15], Time Switched Transmit Diversity (TSTD) [16] and Space-time Transmit Diversity (STTD) [17]. Probably the most commonly noted OL method is the simple Alamouti scheme [18], which is based on STTD and achieves a diversity order of two, the highest possible for a two transmit antenna system. Presentation and comparison of OL techniques incorporated in 3rd generation (3G) systems can be found in [19][20]. A brief description of OL techniques for long term evolution (LTE) can be found in [21].

2.1.3 Closed-Loop Methods

In CL systems, the transmitter requires knowledge of the channel. In such systems, the receiver has the capability to periodically measure the channel and report back to the transmitter, through a specified control channel, information that will help to improve the perceived performance. In general, channel knowledge acquired at the transmitter is imperfect, due to the error-prone, delay-sensitive and capacity-limited nature of the feedback channel.

Extensive research has been carried out for finding efficient ways to convey and optimally utilize partial CSIT through the available control channel. Partial feedback strategies presented in literature typically focus on different characteristics of the real-time feedback channel separately for simplicity. As an example, mean and covariance feedback models [22][23][24] focus on the effects of feedback delay and channel estimation errors, but usually assume that mean and covariance values are fed back in non-quantized form. Similarly, magnitude feedback, which involves sending back information only about the norm of the channel gains [25], assumes that accurate values of the channel norm can be fed back.

From a different perspective, quantized feedback schemes [26][27][28][29][30] are based on the realization that feedback channel capacity is limited. With limited channel capacity for signaling purposes, the design goal of the system is to minimize the uplink overhead and optimize a performance metric at the receiver (e.g. received SNR). Effectiveness of quantized CL feedback schemes depends on the availability, accuracy and update rate of CSIT. Thus, trade-offs between resolution and frequency of feedback must be considered. It has been verified that in fast fading channels, the most critical factor is the frequency of feedback, while in slow-fading channels priority should be given to the resolution of feedback [31].

2.2 Transmit Beamforming and MISO System Model

Transmit beamforming is a processing technique that exploits knowledge of CSIT to optimally adapt the transmit symbols to channel conditions, and enhance performance at the receiver side by altering the transmission radiation pattern. The term 'transmit beamforming' commonly represents a special case of precoding (i.e. single-layer precoding) and can be easiest described using a MISO system
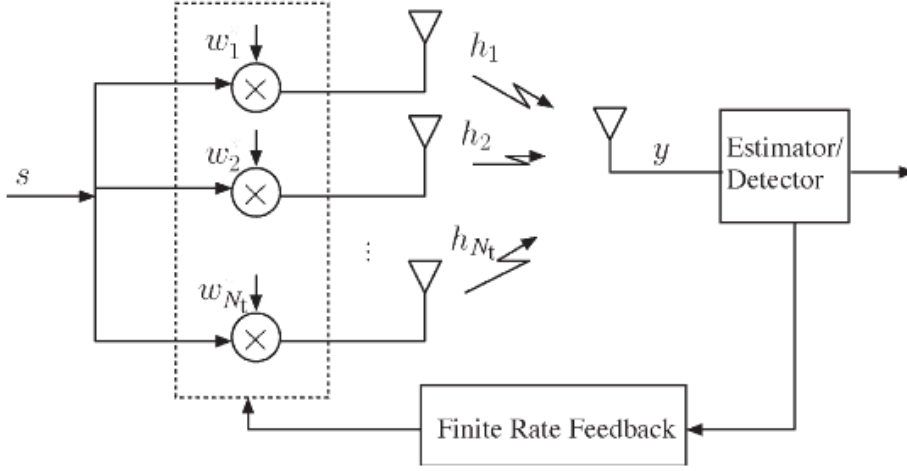
Figure 2.1: Transmit beamforming block diagram. Symbol s is sent through N_t transmit antennas. Prior to transmission, a beamforming weight w_i is applied to the signal of each antenna, according to knowledge obtained from the receiver, through a finite rate feedback channel. At the receiver, the signal y is received.

model. With TBF, a single symbol s is sent through n of the available N_t transmit antennas ($n \leq N_t$) after it has been multiplied by a beamforming vector $\mathbf{w}$ (see Fig. 2.1). The vector channel $\mathbf{h}$ consists of scalar complex weights h_i, each corresponding to the channel between the i-th transmit antenna and the receiver. The beamforming vector $\mathbf{w}$ consists of scalar complex weights w_i, which are chosen based on the feedback information acquired by the receiver. Beamforming vectors need to satisfy $\|\mathbf{w}\| \leq 1$, so that amplifications in the available transmit power are avoided. At the single-antenna receiver, the signal y is received, which is the superposition of the signals from all transmit antennas.

We will assume that the BS is equipped with N_t transmit antennas and the user equipment (UE) with a single receive antenna. Considering single path Rayleigh fading channels, the vector channel is given by $\mathbf{h} = [h_1, h_2, ..., h_{N_t}]$, where h_i are independent and identically distributed (i.i.d.) zero-mean circularly symmetric complex Gaussian random variables (RVs) normalized to unit power. With $E\{|h_i|^2\} = 1$, we have $E\{\|\mathbf{h}\|^2\} = N_t$. Let $\hat{\mathbf{w}} = [w_1, w_2, ..., w_{N_t}]$, with $\|\hat{\mathbf{w}}\| = 1$, be the chosen beamforming vector from a predefined codebook $\mathcal{W}$. For conventional TBF, the goal is to maximize SNR at reception (i.e. egoistic TBF),

thus, $\hat{\mathbf{w}}$ is chosen such that

$$\hat{\mathbf{w}} = \arg\max_{\mathbf{w}\in\mathcal{W}} |\mathbf{h}\cdot\mathbf{w}|. \tag{2.1}$$

Then, the received signal at the target UE is

$$y = (\mathbf{h}\cdot\hat{\mathbf{w}})s + \tilde{n}, \tag{2.2}$$

where $\tilde{n} \in \mathbb{C}$ is zero-mean complex Gaussian noise with noise spectral density N_0.

2.3 Quantized CSIT and Codebook Design Framework

Perfect knowledge of CSIT is unrealistic in practical systems. Hence, the choice of $\mathbf{w}$ is based on quantized information fed back by the receiver at periodic time intervals. In early works [32][33], the receiver quantized the channel itself, and directly designed the optimal beamforming vector to be fed back to the transmitter. It is evident that the performance of such an approach is bounded, since it depends on resolution, which cannot be infinite due to limitations of the feedback channel. A simpler approach is to quantize the set of beamforming vectors, not their actual values. The set of chosen beamforming vectors forms a codebook $\mathcal{W}$, which can be shared among transmitter and receiver prior to transmission. Then, the receiver only needs to send back to the transmitter the index of the beamforming vector that maximizes performance. Typically, the CL procedure for this type of TBF is the following:

1. The receiver, at each time instant, selects the optimal beamforming vector $\mathbf{w}$ from a pre-defined codebook $\mathcal{W}$, with goal to maximize some performance metric.

2. The receiver feeds back the index of the chosen beamforming vector.

3. The transmitter retrieves the actual beamforming vector, corresponding to the index received, from its own copy of codebook $\mathcal{W}$ and applies it for transmission.

Generalized techniques for the design of transmit beamforming codebooks have been proposed in literature through the years. One approach is to think of codebook $\mathcal{W}$ as a collection of lines in the Euclidean $\mathbb{C}^{N_t}$ space and try to

maximize the angular separation among the closest neighboring lines [34]. This formulation of the solution is identical to the well-known *Grassmanian line packing* problem of applied mathematics. A second approach is to build codebooks by using *vector quantization (VQ)* techniques. The idea of VQ is based on maximizing the mean-squared weighted inner product between the optimum and the quantized beamforming vector [35]. The previous techniques assume that codebooks are deterministic and independent of the channel conditions. *Random Vector Quantization (RVQ)*, on the other hand, relies on random codebook generation after each channel fading block. These random codebooks must be known perfectly at both transmitter and receiver. Assuming N_B feedback bits, RVQ generates 2^{N_B} codebook vectors i.i.d. according to the stationary distribution of the best unquantized beamforming vector. A survey of the various codebook design techniques can be found in [8].

Practical CL systems use simple deterministic codebooks that require low overhead. Wideband code division multiple access (WCDMA) was the first mobile system that contained explicit support for CL transmit beamforming methods. Incorporation to the standard was based on the observation that, even with minimal quantized feedback resolution, performance improvements were noticeable [36]. In our analysis, we will consider the generalized UTRA-based CL transmit diversity modes found in [37], namely transmitter selection combining (TSC), generalized mode-1 (g-mode 1) and generalized mode-2 (g-mode 2). The codebooks of these modes do not comply with optimal codebook design, but the performance loss is negligible compared to more complex designs [26][34] for small number of transmit antennas and implementation is straightforward [37].

2.3.1 Transmitter Selection Combining

The simplest codebook design technique is TSC, also referred to as selection diversity transmission (SDT) or transmit antenna selection (TAS) [38]. In this feedback scheme, the beamforming vector contains only one non-zero entry. The only non-zero entry corresponds to the transmit antenna that maximizes the received SNR. Hence, codebook $\mathcal{W}$ has the following form:

$$\mathcal{W} = \{(0, ..., 0, \underset{\text{i}}{1}, 0, ..., 0), \qquad i = 1, \dots, N_t\}, \tag{2.3}$$

where i indicates the position of the non-zero value in the vector. The size of this codebook is equal to the number of available transmit antennas N_t; therefore, the

number of feedback bits needed to enumerate all weights is kept low, and is equal to $\lceil \log_2(N_t) \rceil$. Despite its simplicity, this scheme is sensitive to feedback errors and does not allow full beamforming gains [39].

2.3.2 Generalized Mode 1

This type of TBF scheme involves quantizing the phase angle of the complex channel gain associated with each antenna. The first appearance of this method can be found in [40], as partial phase combining (PPC) for the two transmit antenna MISO case. This approach maintains EGT and aims to pre-adjust the phases of the transmit signals from the different antennas with respect to a reference antenna, so that they combine coherently at the receiver. Quantization of phase adjustments is performed as follows: for N_p available phase feedback bits, 2^{N_p} complex weights are generated. The first antenna is considered as reference. Since all phase adjustments are done against this reference antenna, its phase can be assumed zero. For all remaining antennas, the receiver individually chooses the weight that minimizes the angle separation against the reference antenna. These weights have equal amplitudes and uniform angle separation along the complex plane. The choice of uniform quantization is justified by the fact that the phase of a circular complex Gaussian random variable is uniformly distributed. The method UTRA FDD Mode 1 can be seen as a practical implementation of PPC, for constant size of 2 bits per feedback message. To be exact, in UTRA FDD Mode 1 the feedback message is not a 2-bit concrete word, but the result of interpolation between two consecutive one-bit feedback messages. In [37], the concept of uniform phase quantization is generalized to an arbitrary number of transmit antennas under the name of generalized mode 1 (g-mode 1).

In particular, codebook $\mathcal{W}$ contains all vectors $\mathbf{w} = (\frac{1}{\sqrt{N_t}}, w_2, w_3, ..., w_{N_t})$ with

$$w_i \in \left\{ \frac{e^{-j2\pi n/2^{N_p}}}{\sqrt{N_t}}, \qquad 0 \leq n \leq 2^{N_p} - 1 \right\}, \ i = 2, \ldots, N_t. \qquad (2.4)$$

The total number of bits required for the feedback message is $(N_t - 1)N_p$. The capacity of g-mode 1 was shown in [37] to be clearly better than the capacity of TSC. Algorithm g-mode 1 also benefits from the characteristics of EGT; since there is no requirement for amplitude modifications, more efficient amplifier designs can be implemented [41].

2.3.3 Generalized Mode 2

Generalized Mode 2 ranks some (or all) of the channel gains $\{|h_k|\}_{k=1}^{N_t}$ according to their amplitudes, and adjusts their phases by applying g-mode 1. The transmitter then chooses the amount of power to allocate to each antenna, to favor the better channel conditions. Algorithm g-mode 2 is a suboptimal algorithm, due to the fact that phases and amplitudes are adjusted independently. Its codebook $\mathcal{W}$ contains all vectors $\mathbf{w} = (w_1, w_2, w_3, ..., w_{N_t})$ with

$$w_i \in \left\{ \alpha_k \mathrm{e}^{-j2\pi n/2^{N_p}}, \ k = 1, \ldots, N_t \text{ and } n = 0, \ldots, 2^{N_p} - 1 \right\}, \ i = 1, \ldots, N_t, \quad (2.5)$$

where α_k are the amplitude weights satisfying the condition $\sum_{k=1}^{N_t} \alpha_k^2 = 1$.

We note that for $N_t = 2$ transmit antennas, $N_p = 3$ phase feedback bits and $N_a = 1$ amplitude feedback bit, g-mode 2 resembles UTRA FDD Mode 2. In UTRA FDD Mode 2, amplitudes are chosen as $\alpha_1 = \sqrt{0.8}$ and $\alpha_2 = \sqrt{0.2}$ for the transmit antennas characterized by the strongest and weakest channel gains respectively. These values were obtained through numerical simulations. Exact theoretical values for the optimal amplitude weights of the two-antenna case were found to be $\alpha_1 = \sqrt{0.7735}$ and $\alpha_2 = \sqrt{0.2265}$ in [42]. From this point on, when we refer to g-mode 2 for two antennas, we will assume that the amplitude weights are the optimal ones presented above. It is worth noting that despite its good performance, Mode 2 was later removed from the specifications of UTRA FDD in order to simplify the standard.

2.4 Performance Metrics for CL TBF Schemes

In this thesis, we focus on CL TBF schemes when low-bit rate quantization feedback is available, as described in previous sections. In the MISO case, it is common that the expected SNR gain $\mathcal{G}$ is used as performance measure [36]. Specifically, in MISO system with single path channel $\mathbf{h}$ and beamforming vector $\mathbf{w}$, SNR gain from TBF is defined as:

$$\mathcal{G} = \frac{\mathbb{E}\{|\mathbf{h} \cdot \mathbf{w}|^2\}}{\frac{\mathbb{E}\{\|\mathbf{h}\|^2\}}{N_t}}, \quad (2.6)$$

where $\mathbb{E}\{.\}$ denotes expected value. Since we have considered that $E\{\|\mathbf{h}\|^2\} = N_t$, the expression can be simplified as follows:

$$\mathcal{G} = \mathbb{E}\{|\mathbf{h} \cdot \mathbf{w}|^2\}. \quad (2.7)$$

The gain from TBF can also be viewed from the spectral efficiency perspective. Using Jensen's inequality,

$$\mathbb{E}\{\log_2(1 + |\mathbf{h} \cdot \mathbf{w}|^2)\} \leq \log_2(1 + \mathbb{E}\{|\mathbf{h} \cdot \mathbf{w}|^2\}) = \log_2(1 + \mathcal{G}), \qquad (2.8)$$

so $\mathcal{G}$ determines the upper bound for the rate improvement that CSIT introduces. Another common method for illustrating the performance of CL methods is outage probability. Outage probability is defined as the probability that the channel is unable to support a rate of transmission R_{out} (or the corresponding $SINR_{out}$, since these terms are directly connected). If we assume TBF, rate outage probability is given by

$$P(R < R_{out}) = P\left\{\log_2(1 + |\mathbf{h} \cdot \mathbf{w}|^2) < R_{out}\right\}, \qquad (2.9)$$

and SINR outage probability is given by

$$P(SINR < SINR_{out}) = P\left\{|\mathbf{h} \cdot \mathbf{w}|^2 < SINR_{out}\right\}. \qquad (2.10)$$

17

Chapter 3

Interference Management in Two-tier HetNets

The shift towards overlaid co-channel network deployments has introduced further challenges in the management of interference present in future networks. Various techniques have been proposed for limiting the effect of cross-layer interference. The most important interference management schemes include open access mechanism for FBSs, power control for FBSs, resource partitioning between different layers, advanced receivers with interference cancellation capabilities, cooperative transmissions between geographically separated BSs and multi-antenna techniques.

3.1 Open Access Control Mechanism for Femto Cells

Open access mechanism for femto cells is usually disregarded in heterogeneous scenario modeling due to security reasons, limited backhaul bandwidth and sharing concerns of owners. Despite its low popularity, the presence of open access FBSs would immediately alleviate most of the interference problems that accompany closed access. Theoretical studies [43] have shown that open access does not pose a negative impact on the interference conditions of a heterogeneous network, when compared to conventional macro single-layer deployments. In fact, it is deduced that network capacity can increase linearly when open access FBSs are deployed in multi-tier networks. In [44], the dominance of open against closed access is highlighted through simulations, which illustrate that open access can

boost the total cell throughput by 15 % compared to closed access. The observed results can be justified intuitively. With open access, users would simply hand over their connections to the strongest base station and no dead zones would be created. As a consequence, the new optimal connections would lower the transmission powers for the uplink and downlink directions in all base stations of the multi-tier network. All these advantages would come at the cost of the extra signaling, and the possible reduction in the performance of the femto cell user, since resources would no longer be dedicated [45].

3.2   Power Control

Deployment of femto cells in CSG access method under co-channel operation with the macro cell causes coverage holes in the macro layer. Several downlink *power control* (PC) mechanisms have been investigated to combat the presence of dead coverage zones, mainly through adjustments of the transmit powers at the FBS, either in a fixed or dynamic way [46]. The basic requirement is to limit the femto coverage so that interference towards macro users is decreased, but at the same time performance at the served femto UEs is not devastated.

Typically, FBSs set their transmit power after initial start-up, by sensing the surrounding RF conditions, such as the neighbor FBSs list or the macro cell coverage. Fixing the FBS node transmit power to its maximum allowed value is not considered a good option and has already been disregarded [46]. In that particular technical report, it is proposed that the FBS transmit power should be settable from the maximum capable value down to a level of 0 dBm. This procedure can even be assisted by global positioning system (GPS) receivers in the FBS, through a mapping between maximum transmit power and number of detected satellites or reception quality [47]. More specifically, if the FBS is unable to detect a sufficient number of satellites, it can be deduced that it is well within the building area and, thus, well isolated. Then, it can set its transmit power to a higher level and still not pose a significant threat to MUEs lying outside the building.

In general, it has been shown that fixed power does not provide good results in all deployment scenarios, and that adaptive calibration of the transmit power should be considered [7]. Calibration of FBS transmit power provides a method to adaptively modify femto coverage, depending on the macro cell interference levels [48]. The algorithm behind power calibration is based on measurements
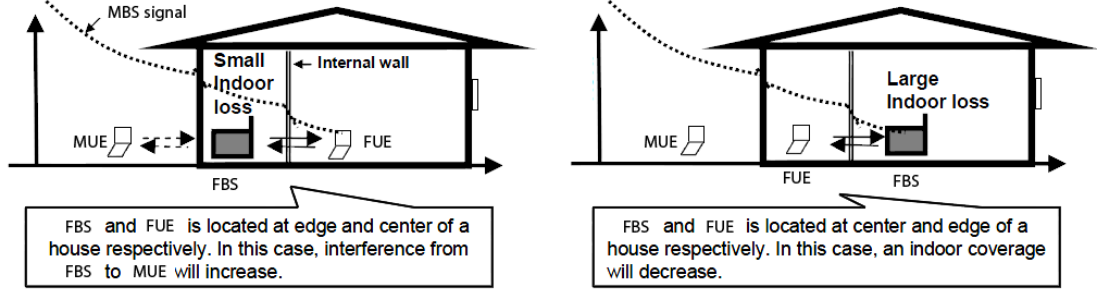
Figure 3.1: Macro-femto cross-layer interference when transmit power in FBS is not properly set [47]. In the left picture, the FBS is closer to the MBS so it sets its transmit power to a higher level. This results to a wider indoor coverage area, but also produces more interference to the MUE. In the right picture, the FBS is further away from the MBS so it sets its transmit power to a lower level. This results to narrower indoor coverage area but also decreases interference to the MUE.

done at the FBS, and involves assessing the received signals from the MBS and other FBSs so that the general interference picture is drawn. In some cases, though, the conditions experienced by femto and macro users might not coincide with those observed by the femto (see Fig. 3.1). Thus, further assistance from the users might be useful so that samples from different locations in the coverage area are provided. This can be done through explicit feedback in the uplink, estimation of the FBS-MUE path loss [49], or even through the failed attempts of the MUE to access the CSG femto cell [48].

3.3 Resource Partitioning

Dividing the resources between macro and femto cells is an effective measure against cross-layer interference. *Resource partitioning* can be performed both in frequency and time domains, in a static, semi-dynamic or completely dynamic way [50]. So far, most partitioning schemes regarding two-tier deployments focus on the frequency domain, due to the fact that resource partitioning in the time-domain requires standardized mechanisms for time synchronization among the different layer transmitters, and this is considered a difficult task [50].

The simplest approach is to divide the total available spectrum into multiple non-overlapping carriers, and assign a subset of these carriers to the macro layer, and the remaining carriers to the femto layer. This approach also applies for
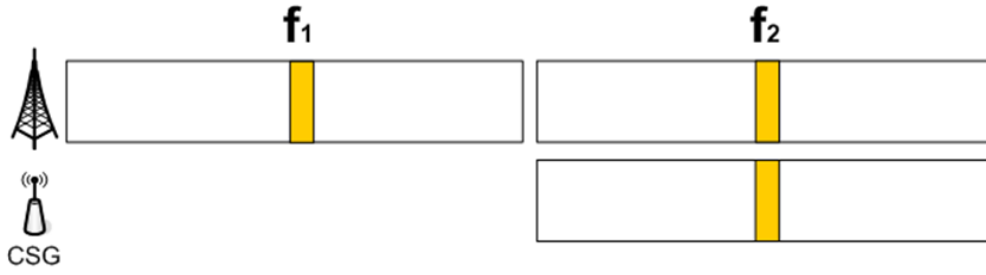
Figure 3.2: Resource partitioning using an escape carrier [52]. The macro layer can use either
carrier f_1 or f_2, but the femto layer is restricted to f_2. When an MUE, which operates on
carrier f_2, approaches an FBS, it senses high interference and attempts to switch to the escape
carrier f_1 where it experiences no interference.

the case of splitting a single carrier in multiple subbands. In [51], the authors
propose an algorithm for the optimal orthogonal spectrum allocation between
macro and femto cells, and also for further splitting of the dedicated femto band
among the individual femto cells. This orthogonal resource partitioning scheme
eliminates cross-layer interference completely, but its drawback is that it reduces
the spectrum usage efficiency for the operator.

Due to the inefficiency and cost of such a scheme, proposals that consider some
form of frequency reuse have been extensively investigated. One approach is the
use of two carriers, the first of which serves as an escape carrier [52]. Consider
carriers f_1 and f_2 as shown in the Fig. 3.2.

In this case, both f_1 and f_2 carriers are assigned to the macro cell layer, but
only f_2 is assigned to the femto cell layer. When MUEs, which are assigned to the
f_2 carrier, sense high cross-layer interference from the transmission of a nearby
FBS, they will automatically issue a request for handover to the escape carrier
f_1. This type of cross-layer interference mitigation is most attractive when the
deployment density of the FBSs is moderate. For dense FBS environments, this
method should be used in conjunction with PC. A variation of this approach is
dynamic carrier selection at each FBS, in which different FBSs are allowed to
choose either f_1 or f_2 as their carrier. Determination of the carrier frequency
could be random or based on measurements of neighboring interferer FBSs. This
approach primarily aims to leverage the co-layer interference between the FBSs,
but gains experienced by inter-frequency handover of interfered MUEs still exist,
even though they are not as high as in the static carrier allocation case.

Various other schemes involving resource partitioning have been presented in

the academic and industrial literature. In [53], the direction of arrival (DoA) of the MUE is compared to the direction range of the FBS, and the result determines the type of scheduling that will be used. If the MUE is not in the direction range of the FBS, it can use any of the available frequencies. Otherwise, the scheduling priority of the frequency resources used by the FBS is set to a lower value, in order to decrease the cross-layer interference towards the MUE. In [54], the macro cell layer frequency resources are partitioned into contiguous non-overlapping sub-bands under the fractional frequency reuse scheme (FFR), in which one subband is assigned to the cell center zone and the remaining subbands are assigned to the cell edge zone. The center band adopts a reuse factor of one, while the edge bands adopt a larger reuse factor. For each subband, a different macro transmit power is chosen. The claim of [54] is that such subband partitioning not only improves the rates of the macro cell users, but also provides opportunities for simultaneous femto cell transmissions through the same frequency resources, without emission of extensive interference to the macro cell layer. In [55], the MBS senses when a served MUE is in the vicinity of a high-interference femto cell and it dynamically determines a set of resources that the FBS should restrict its transmission to. This restriction message is then relayed through the MUE to the interferer FBS.

3.4 Successive Interference Cancellation

Successive interference cancellation (SIC) techniques have already been implemented in 3G systems, and aim to exploit the structure of the interference through reconstruction of the dominant interference signals and subtraction from the total interference [56]. With SIC, the dominant interferer is the first to be detected and decoded, due to its high received power when compared to the remaining interfering signals. Using accurate channel gain estimation, the decoded version of the interfering signal is regenerated in such a way that it resembles the actual received signal, and is then subtracted from the composite received signal. This procedure can be repeated for the remaining interferers. After each step, the next user to be decoded faces less and less interference. Usage of SIC alone is not as effective in heterogeneous deployments, due to differences in cross-layer synchronization and opportunistic placements of femto nodes [57].

3.5   Coordinated Multi-Point Transmission

Recently, a lot of emphasis has been given on so-called coordinated transmission methods that could minimize inter-cell interference. *Coordinated Multi-point* (CoMP) [58][59][60] is a technique, incorporated in 3GPP LTE-Advanced, whose purpose is to exploit or avoid co-channel interference and enhance primarily cell-edge user throughput between MBSs. Improving the signal strength at cell edge implies improving the interference situation of the whole two-tier deployment.

Downlink CoMP strategies require the cooperation of geographically separated base stations, for determining the transmission scheme that will jointly optimize performance among their corresponding UEs. In CoMP, procedures of beamforming, scheduling and data transmission are performed jointly in an explicit manner between collaborating nodes. Architectures of CoMP can be either

1. centralized or

2. distributed,

depending on how UE feedback is shared among the transmission points. Both architectures support two schemes for the coordination of the transmission points; for downlink, CoMP schemes are divided into

1. Joint Processing (JP) and

2. Cooperative Scheduling/Beamforming (CS/CB).

Centralized architecture demands the presence of a central unit (CU), which is responsible for gathering and processing CSIT information from all individual UEs served by a cluster of cooperating MBSs. The cooperating MBSs are connected to the CU in star topology via low-latency backhaul links, such as optical fiber. These links carry signaling overhead and allow the cluster of MBSs to behave as a single entity. Assuming FDD operation, UEs need to estimate CSIT information regarding each MBS of the coordination cluster and report it to their own serving (anchor) MBS. Each anchor MBS forwards the information received to the central unit. Thus, global CSIT is only available at the CU. The CU jointly processes the received CSI information to decide the scheduling of users and the precoding parameters that each MBS should use. Finally, the CU forwards to each MBS the chosen precoding parameters and transmission begins.

Distributed architecture was proposed in [61] to alleviate the challenges present in the centralized architecture. In distributed architecture, the CU is completely

removed and backhaul links that connect MBSs are not necessary, since there is no need for direct exchange of signaling or data information among MBSs anymore. The benefit of a distributed approach is that deployment does not stray too much from that of conventional systems, so only minimal changes are required for adaptation. The simplification of the architecture introduces changes in the framework. Firstly, UEs do not send feedback only to their anchor MBS, but to each MBS of the coordination cluster. Secondly, the burden of scheduling and precoding is shifted to each MBS. Thus, it is important that the scheduling algorithms, which are performed independently at each MBS, are identical.

In JP, data towards a UE is shared among the cooperating MBSs. This scheme exploits the low correlation of the geographically separated sites to improve the data transmission. Transmission can be either coherent or non-coherent, depending on whether phase information feedback is available to combine the signals at the receiver or in an opportunistic way. Joint processing offers two different approaches for transmission of data. With joint transmission (JT), data transmission can be performed simultaneously by multiple MBSs. With dynamic cell selection (DCS), fast dynamic scheduling is executed, usually on a subframe-per-subframe basis, and a single MBS is chosen to transmit data. This MBS can be different from the anchor MBS of the UE. Schemes based on JP can offer large performance gains, particularly for cell-edge users.

In CS/CB, only the anchor MBS has access to data of its served UE. This scheme requires coordination of user scheduling and beamforming among the MBSs of the cluster in order to enhance sum data rates and reduce interference. Theoretically, CS/CB is always outperformed by JP, since the former aims to avoid interference while the latter exploits interference and converts it to useful signal. When the capacity limit of the backhaul is taken into account, though, it has been observed that CS/CB can produce better results than JP [62]. A more thorough presentation of CoMP architectures and transmission schemes can be found in [61][63][64][65].

3.6 Altruistic Beamforming

Altruistic Beamforming is a technique, first presented in [66], which boosts the performance of a badly interfered UE by borrowing degrees of freedom from a subset of its interferers. Although this technique was presented in the context of co-layer femto interference, it can be directly adopted to cross-layer interference

scenarios involving a highly interfered MUE and multiple FBS interferers. Altruistic beamforming can be utilized in downlink cross-layer interference scenarios that involve an MUE located in the vicinity of multiple FBSs, which operate simultaneously with fixed transmit power. Initially, it is assumed that all transmitters apply transmit beamforming in an egoistic manner, having as goal to maximize the perceived rates of their own users. This results to severe degradation of the SINR received at the MUE. In order to decrease the received cross-layer interference, the MUE establishes a control connection with a subset of its dominant interferers and proposes that they change their beamforming vectors such that power leakage is steered away from the MUE. When this procedure is followed by multiple dominant FBSs, the quality of the MBS-MUE link is enhanced, since the total interference is decreased significantly.

The main tool used in Altruistic Beamforming are the modified TBF methods (i.e. TSC, g-mode 1, g-mode 2) which were previously presented in section 2.3. These methods can be adapted to combat interference without alteration of their codebooks. The MBS acts always in an egoistic manner, deciding its beamforming vector $\hat{\mathbf{w}}$ from codebook $\mathcal{W}_m$ according to equation

$$\hat{\mathbf{w}} = \arg \max_{\mathbf{w} \in \mathcal{W}_m} |\mathbf{h_m} \cdot \mathbf{w}|, \tag{3.1}$$

where $\mathbf{h_m}$ denotes the channel between MBS and MUE. In contrast, each interferer FBS substitutes the applied egoistic beamforming vector with the altruistic one that minimizes interference, i.e. the optimal beamforming vector $\check{\mathbf{w}}$ for an altruistic interferer FBS is now chosen from codebook $\mathcal{W}_f$ according to

$$\check{\mathbf{w}} = \arg \min_{\mathbf{w} \in \mathcal{W}_f} |\mathbf{h_f} \cdot \mathbf{w}|, \tag{3.2}$$

where $\mathbf{h}_f$ now denotes the interference channel between FBS and MUE. It should be noted that the FBS is not given a choice of different beamforming vectors for interference mitigation, but can only use the beamforming vector that minimizes interference. A scheme for providing the FBS with multiple feedback weights was presented in [67], where the victim MUE feeds back a list of candidate beamforming vectors and the FBS chooses the beamforming vector that degrades performance as little as possible for its own FUE. In this thesis, we consider that the MUE is not in a position to bargain, but needs all the help it can be offered; therefore, only the minimizing beamforming vector is fed back.

The trade-off for the SINR improvement at the interfered MUE is the loss of beamforming gain at each FBS, as implied by usage of the term 'altruistic'. After

applying the MUE-proposed beamforming vector, FBSs do not take into account the fast fading effect due to the randomness of the underlying wireless channel. This tolerance on the degradation of femto cell performance can be well justified; from the point of view of the operator, the macro cell is modeled as primary infrastructure, since it promises ubiquitous coverage and is responsible for serving a large number of subscribers [68]. From the performance side, the mean loss from beamforming is not significant, since the channel conditions experienced by femto users are usually above average. Indeed, indoor deployment assures a low attenuation environment, which is shielded against outdoor signals by means of thick walls. Furthermore, minimum distance between FBS and FUE has been set equal to 0.2 m [69]; therefore, it can be also assumed that FUEs are as close to the FBS as needed to experience excellent channel conditions.

Chapter 4

Generalized System Model

The general layout of our heterogeneous system model is shown in Fig. 4.1. The network comprises of an MBS and a group of indoor FBSs, which operate in the same frequency band. The FBSs are concentrated in a 5-by-5 apartment grid, and each apartment is modeled as a square with no doors or windows. This type of model was proposed in [69]. We consider that each apartment occupies an area of $15{\times}15\text{m}^2$. It is assumed that FBSs are installed in a subset of the apartments and, for simplicity, their location is fixed at the center of each apartment. Furthermore, FBSs operate simultaneously under CSG configuration, serving one user each.

The studied interference scenario involves a user who is placed at a specific location, 5m from the right wall and 7m from upper wall inside the central apartment of the block of flats. It is assumed that the user has not installed an FBS at the specified apartment and, therefore, has no choice but to connect to the macro BS. In such a scenario, the MUE is bound to receive a great amount of interference from the surrounding FBSs and a weakened, but still acceptable, signal from its serving MBS due to the additional wall penetration losses.

4.1   Adopted Assumptions

In our system model, the following assumptions have been made:

1. The block of flats is located sufficiently close to the macro cell center. Since the block of apartments is far from the cell edge, interference from other MBSs is overshadowed by interference from the FBS cluster (i.e. single MBS system model).
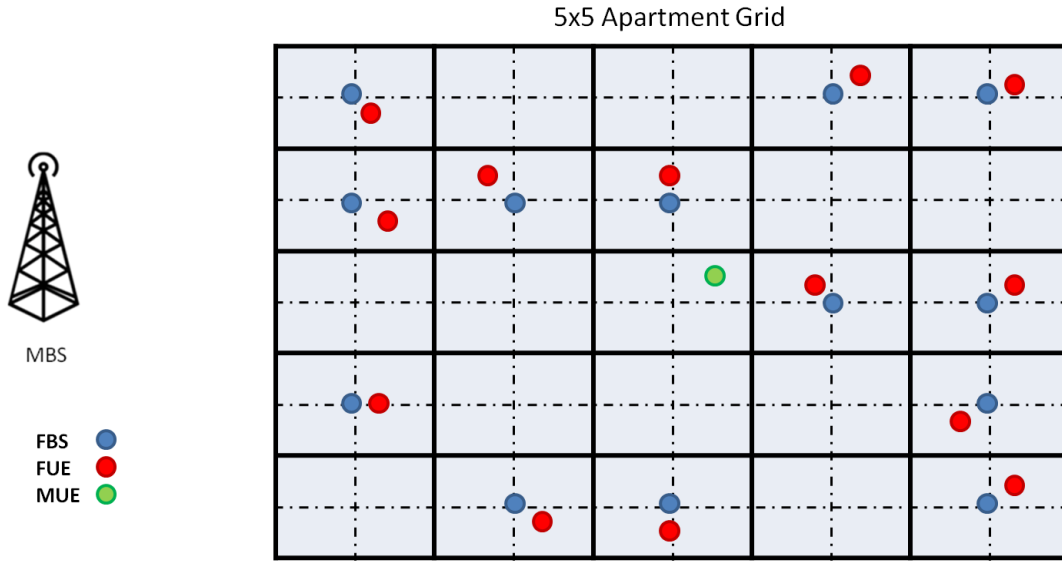
Figure 4.1: The system model comprises of a single MBS-MUE pair and multiple FBS-FUE pairs. The FBSs are located inside a 5-by-5 apartment grid, at the center of apartments (blue dots). All FUEs are randomly placed and experience very good channel conditions from their serving FBS (red dots). The MUE is located in the central apartment (green dot), where no FBS is available.

2. Each transmitter possesses 2 transmit antennas and each receiver a single receive antenna (i.e. MISO system model). Channel gains related to different antennas of the same MBS/FBS are modeled as i.i.d. zero-mean circularly symmetric complex Gaussian RVs. Their values remain constant over the duration of a block, and change independently between contiguous blocks. Both MBS and FBSs transmit with constant power. Transmit power of different FBSs is equal.

3. Transmissions are performed in FDD mode. The victim MUE is able to perfectly estimate the downlink channels from the FBS interferers and can establish low-rate, over-the-air and on-demand control connections for exchange of instantaneous channel information with a subset of them.

4. It is assumed that co-layer interference leakage between femto cellular networks and cross-layer leakage between macro and femto cellular networks do not deteriorate the very good channel conditions of the individual femto networks significantly.

5. The impact of feedback delay and signaling errors is ignored. Focus is given

on the quantization aspect of the feedback channel.

We remark that extension of the analysis to support multiple MUEs is straightforward. In the case of single carrier HSDPA, different MUEs can be scheduled in time in the shared channel, so that the altruistic behavior of the FBSs can change accordingly between transmission time intervals (TTIs) to fit the needs of each MUE. In the case of LTE and LTE-Advanced, hard frequency reuse can be applied, and MUEs can be scheduled to receive in non-overlapping parts of the spectrum, since OFDMA is used as air interface.

4.2 Mean and Instantaneous SINR at the MUE

Let $\mathcal{S}$ denote the set comprising of all FBSs interferers from the perspective of the MUE. Consider the ordered set $\mathcal{S}_A \subseteq \mathcal{S}$, containing those FBSs that apply altruistic TBF to mitigate instantaneous interference at the MUE. The ranking is performed from strongest to weakest interferer, taking into account only their large scale fading statistics. Order is important, since our aim is to mitigate the fast fading term of the first k strongest interferers, to provide the highest possible performance gains. The set $\mathcal{S}_E \subseteq \mathcal{S}$, which is the complement of $\mathcal{S}_A$, contains the remaining FBSs that perform egoistic TBF to favor their own FUEs. The mean received power of all egoistic FBSs with indices $i \in \mathcal{S}_E$ is grouped together with thermal noise power and treated as background interference. Therefore, order is not important for $\mathcal{S}_E$.

The MBS transmits with constant transmit power P_m and all FBSs with constant transmit power P_f. The distance dependent path loss between MBS and MUE is denoted as L_m, while L_{f_i} ($\forall i \in \mathcal{S}$) denotes the distance dependent attenuation between altruistic FBS$_i$ and MUE. Thermal noise power is denoted as P_n. The mean received SINR at the MUE can then be represented as

$$
\begin{aligned}
\overline{\text{SINR}}_{\text{mue}} &= \frac{\frac{P_m}{L_m}}{P_n + \sum\limits_{i \in \mathcal{S}_E} \frac{P_f}{L_{f_i}} + \sum\limits_{i \in \mathcal{S}_A} \frac{P_f}{L_{f_i}}} = \frac{\frac{P_m}{L_m}}{P_I + \sum\limits_{i \in \mathcal{S}_A} \frac{P_f}{L_{f_i}}} \\
&= \frac{\frac{P_m}{P_I L_m}}{1 + \sum\limits_{i \in \mathcal{S}_A} \frac{P_f}{P_I L_{f_i}}} = \frac{\bar{\gamma}_m}{1 + \sum\limits_{i \in \mathcal{S}_A} \bar{\gamma}_{f_i}}.
\end{aligned}
\tag{4.1}
$$

where $\bar{\gamma}_m$ and $\bar{\gamma}_{f_i}$ denote the mean received SINR at the MUE, from the MBS and each FBS$_i$ respectively, when signals from egoistic users and thermal noise are

forming the interference P_I. Due to the definition of $\mathcal{S}_A$, the term $\bar{\gamma}_{f_1}$ represents the strongest interferer.

For the modeling of the instantaneous SINR at the MUE, we consider the fast fading component in the egoistic MBS and the altruistic FBSs. Then, the channel between MBS and MUE is $\mathbf{h_m} = [h_{m,1} \ h_{m,2}]$, and the egoistic beamforming vector applied is given by (2.1). Similarly, the channel between altruistic FBS$_i$ and MUE is $\mathbf{h_{f_i}} = [h_{f_i,1} \ h_{f_i,2}]$ and the beamforming vector applied by FBS$_i$ is given by (3.2). The instantaneous SINR at the MUE is, then, given by

$$\text{SINR}_{\text{mue}} = \frac{\bar{\gamma}_{\text{m}}|\mathbf{h_m} \cdot \hat{\mathbf{w}}_{\mathbf{m}}|^2}{1 + \sum\limits_{i \in \mathcal{S}_{\text{A}}} \bar{\gamma}_{\text{f}_i}|\mathbf{h_{f_i}} \cdot \check{\mathbf{w}}_{\mathbf{f_i}}|^2}. \tag{4.2}$$

4.3 System Parameters

Table 4.1: Simulation Parameters

Parameter	Value
System Parameters	
Carrier Frequency	2 GHz
Bandwidth	5 MHz
Thermal Noise PSD	-174 dBm/Hz
UE Noise Figure	7 dB
Inner Wall Penetration Loss (L_{iw})	5 dB
Outer Wall Penetration Loss (L_{ow})	20 dB
MBS Parameters	
MBS Tx Power	46 dBm
MBS Antenna Gain	18 dBi
Cable Losses	5 dB
FBS Parameters	
FBS Tx Power	10 dBm
FBS Antenna Gain	0 dBi

To calculate the varying $\bar{\gamma}_m$, $\bar{\gamma}_{f_i}$ parameters, we carry out simulations based on the parameters of Table 4.1. To calculate the path loss attenuation, we consider

the path loss models presented in [69]. For indoor-initiated transmissions (i.e. FBS to FUE and FBS to MUE) the path loss model is given by:

$$PL_{in}(dB) = 38.46 + 20log_{10}R + 0.7d_{2D,in} + 18.3n^{((n+2)(n+1)-0.46)} + q \cdot L_{iw},$$

where R is the distance in meters between transmitter and receiver, $d_{2D,in}$ is the part of this distance which is indoors, n is the number of floors that separate transmitter and receiver, L_{iw} is the penetration loss of inner walls and q is the number of penetrated indoor walls that the signal must pass through. We will study single floor cases, therefore $n = 0$. Also, all UEs will reside indoors, therefore $R = d_{2D,in}$. For outdoor-initiated transmissions (i.e., MBS to FUEs and MBS to MUE), the path loss model is given by

$$PL_{out}(dB) = 15.3 + 37.6log_{10}R + L_{ow} + q \cdot L_{iw},$$

where the term L_{ow} refers to outer wall penetration loss.

4.4 Probabilistic Modeling of Instantaneous Received SINR

The received instantaneous SINR of the MUE can be represented as an RV which is a function of multiple RVs, i.e.

$$Z = \frac{X}{1 + \sum_{i \in \mathcal{S}_A} Y_i}, \tag{4.3}$$

where $X = \bar{\gamma}_m |\mathbf{h_m} \cdot \hat{\mathbf{w}}_{\mathbf{m}}|^2$ and $Y_i = \bar{\gamma}_{f_i} |\mathbf{h_{f_i}} \cdot \check{\mathbf{w}}_{\mathbf{f_i}}|^2$.

In following chapters, we will present analytical expressions for the cumulative distribution function (CDF) of Z, denoted as $F_Z(z)$. Another illustration of the downlink performance of the MUE is the outage probability of its spectral efficiency (or rate distribution), which is directly obtained using $F_Z(z)$. It is well known that downlink rate is a function of the received SINR, and specifically $R = \log_2(1 + Z)$. The CDF $F_R(r)$ of R can be given in terms of $F_Z(z)$ as follows:

$$F_R(r) = F_Z(2^r - 1). \tag{4.4}$$

Chapter 5

Perfect Phase Altruistic Beamforming

In this chapter, we assume that capacity for the CL feedback link is unrestricted, and we apply g-mode 1 to mitigate the effect of one dominant FBS interferer. With perfect channel phase information fed back to the transmitter, the optimal EGT weights can be applied and signals can be combined perfectly at the receiver. For the 2x1 MISO case, the signals sent from the antennas of the MBS, which carry the same symbol, combine with zero phase difference at the receiver, while the interference signals from the dominant FBS combine in exactly opposite phases (see Fig. 5.1).
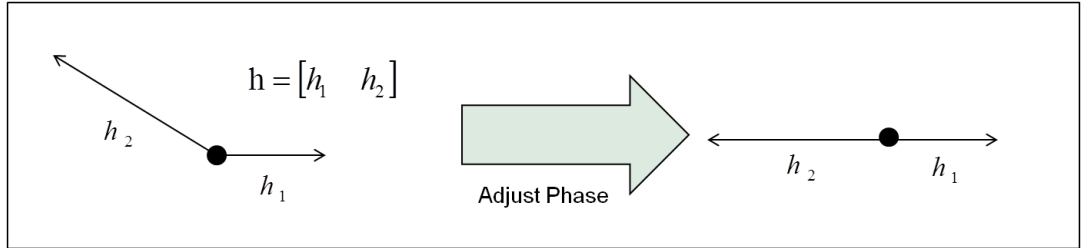
Figure 5.1: In the case of unrestricted phase feedback,channel gains of the interfering signals can be oriented in such a way that their phase difference is 180 degrees.

The purpose of this study is to deduce the analytical upper bound for the performance of the interfered MUE user under g-mode 1, in the 2x1 MISO case with one dominant FBS interferer. Then, the performance of low-resolution quantized feedback can be measured against this upper bound. To justify the claim of one dominant interferer in the proposed system model, we assume that only one of the adjacent apartments contains an FBS which is transmitting (Fig. 5.2). We
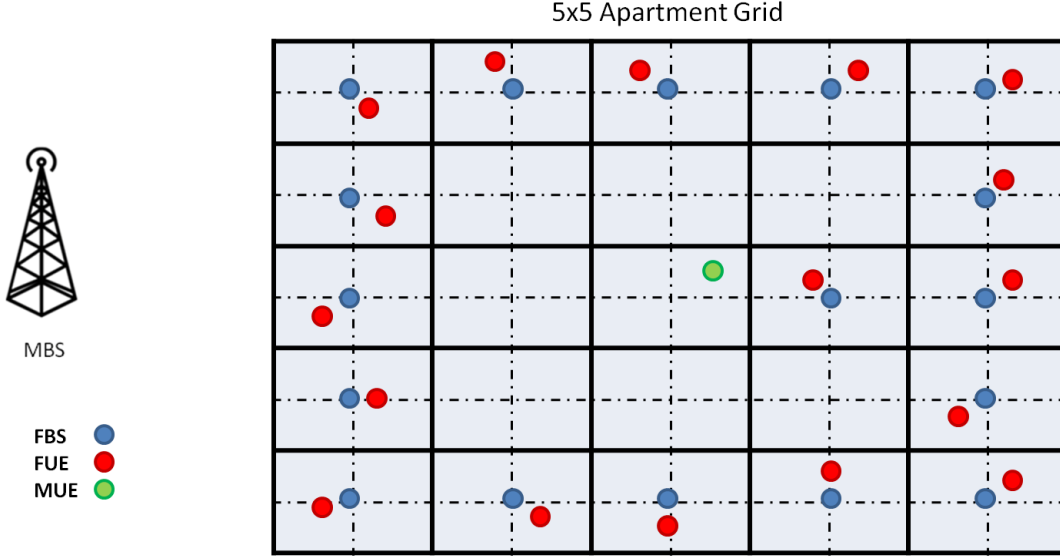
Figure 5.2: The system model comprises of a single MBS-MUE pair and 17 FBS-FUE pairs. Only a single dominant interferer FBS is identified by the MUE, originating from the only adjacent apartment that contains an FBS.

note that the analysis is not restricted to the proposed system model, but can be directly applied to cases where the assumption of one dominant interferer is well justified.

5.1 Received SINR with Unrestricted Phase Feedback Resolution

Let $\mathbf{h} = [h_1 \; h_2]$, with $h_1 = |h_1|e^{j\angle h_1}$ and $h_2 = |h_2|e^{j\angle h_2}$, be the channel gain vector related to BS transmit antennas 1 and 2, respectively, and let $\mathbf{w} = [w_1 \; w_2]$, with $w_1 = |w_1|e^{j\angle w_1}$ and $w_2 = |w_2|e^{j\angle w_2}$, be the corresponding complex beamforming weights per transmit antenna. We assume that h_1 and h_2 are complex zero-mean Gaussian i.i.d. RVs with unitary variance. Beamforming vectors $\mathbf{w}$ satisfy $\|\mathbf{w}\| = 1$. The received instantaneous SNR at the target UE will then

be

$$
\begin{aligned}
|\mathbf{h} \cdot \mathbf{w}|^2 &= |h_1 w_1 + h_2 w_2|^2 \\
&= (h_1 w_1 + h_2 w_2)(h_1^* w_1^* + h_2^* w_2^*) \\
&= h_1 w_1 h_1^* w_1^* + h_1 w_1 h_2^* w_2^* + h_2 w_2 h_1^* w_1^* + h_2 w_2 h_2^* w_2^* \\
&= |h_1|^2 |w_1|^2 + |h_2|^2 |w_2|^2 + 2\operatorname{Re}\{h_1 w_1 h_2^* w_2^*\} \\
&= |h_1|^2 |w_1|^2 + |h_2|^2 |w_2|^2 + 2\operatorname{Re}\{|h_1| e^{j\angle h_1} |w_1| e^{j\angle w_1} |h_2| e^{-j\angle h_2} |w_2| e^{-j\angle w_2}\} \\
&= |h_1|^2 |w_1|^2 + |h_2|^2 |w_2|^2 + 2|h_1||h_2||w_1||w_2| \cos\{\angle h_1 + \angle w_1 - \angle h_2 - \angle w_2\}.
\end{aligned}
$$
(5.1)

Without loss of generality, we can assume that $h_1 \in \mathbb{R}$, since we are interested in the relative phase of the two antennas. Then $\angle h_1 = \angle w_1 = 0$. In g-mode 1, power is distributed equally among antennas, i.e., $|w_1| = |w_2| = \frac{1}{\sqrt{2}}$. Then,

$$
|\mathbf{h} \cdot \mathbf{w}|^2 = \frac{1}{2}|h_1|^2 + \frac{1}{2}|h_2|^2 + |h_1||h_2| \cos\{-\angle h_2 - \angle w_2\}.
$$
(5.2)

In order to maximize (5.2), the condition $\angle w_2 = -\angle h_2$ should be satisfied. Then,

$$
\text{SNR}_{\max}^{\text{g-mode 1}} = |\mathbf{h} \cdot \mathbf{w}|_{\max}^2 = \frac{1}{2}|h_1|^2 + \frac{1}{2}|h_2|^2 + |h_1||h_2| = \frac{1}{2}(|h_1| + |h_2|)^2.
$$
(5.3)

Similarly, to minimize (5.2), the condition $\angle w_2 = -\angle h_2 + \pi$ should be satisfied. Then,

$$
\text{SNR}_{\min}^{\text{g-mode 1}} = |\mathbf{h} \cdot \mathbf{w}|_{\min}^2 = \frac{1}{2}|h_1|^2 + \frac{1}{2}|h_2|^2 - |h_1||h_2| = \frac{1}{2}(|h_1| - |h_2|)^2.
$$
(5.4)

Equations (5.3) and (5.4) constitute upper and lower bounds of SNR when equal power is distributed to both transmit antennas. In order to obtain the above equations, h_1 and h_2 must be fully aligned; therefore, phases of weights w_1 and w_2 are required to take continuous values in the interval $(-\pi, \pi)$. This can be realizable with g-mode 1 only theoretically, if the number of phase feedback bits tends to infinity (i.e. when $N_p \to \infty$).

In an interference scenario with one dominant FBS interferer, the received SINR of the MUE under g-mode 1 with infinite number of feedback bits is given by

$$
\text{SINR}_{\text{mue}}^{\max} = \frac{\bar{\gamma}_{\text{x}} |\mathbf{h}_{\mathbf{x}} \cdot \hat{\mathbf{w}}_{\mathbf{x}}|_{max}^2}{1 + \bar{\gamma}_{\text{y}} |\mathbf{h}_{\mathbf{y}} \cdot \check{\mathbf{w}}_{\mathbf{y}}|_{min}^2}.
$$
(5.5)

Parameter $\bar{\gamma}_{\text{x}}$ denotes the mean SINR received from the MBS, while $\bar{\gamma}_{\text{y}}$ denotes the mean SNR received from the dominant FBS considering thermal noise and

signals from egoistic interferers as background interference. Vector $\mathbf{h_x} = [\mathrm{h_{x1}} \; \mathrm{h_{x2}}]$ expresses the channel between MBS and MUE, while $\mathbf{h_y} = [\mathrm{h_{y1}} \; \mathrm{h_{y2}}]$ corresponds to the channel between dominant FBS and MUE. Vector $\hat{\mathbf{w}}_\mathbf{x} = [\hat{\mathrm{w}}_{\mathrm{x1}} \; \hat{\mathrm{w}}_{\mathrm{x2}}]^T$ is the beamforming vector applied by the MBS to maximize the wanted SNR at the MUE, while $\check{\mathbf{w}}_\mathbf{y} = [\check{\mathrm{w}}_{\mathrm{y1}} \; \check{\mathrm{w}}_{\mathrm{y2}}]^T$ is the beamforming vector applied by the dominant FBS to minimize interference at the MUE.

In order to measure the performance of the received SINR, we will derive the CDF of the RV

$$Z = \frac{X}{1+Y}, \tag{5.6}$$

with $X = \bar{\gamma}_\mathrm{x}|\mathbf{h_x} \cdot \hat{\mathbf{w}}_\mathbf{x}|^2_{max}$ and $Y = \bar{\gamma}_\mathrm{y}|\mathbf{h_y} \cdot \check{\mathbf{w}}_\mathbf{y}|^2_{min}$ positive independent RVs.

5.2   Probability Distribution for Desired Signal

In this section, we present the probability density function (PDF) and CDF of

$$X = \bar{\gamma}_\mathrm{x}|\mathbf{h_x} \cdot \hat{\mathbf{w}}_\mathbf{x}|^2_{max} = \frac{\bar{\gamma}_\mathrm{x}}{2}(|\mathrm{h_{x1}}| + |\mathrm{h_{x2}}|)^2, \tag{5.7}$$

which is the squared sum of two independent Rayleigh RVs (see $(A.2) - (A.4)$ in Appendix A), scaled by a constant factor. Derivation of the PDF of X was performed using the procedure found in [70] for determining the PDF of an RV which is a function of multiple RVs. We apply this procedure step-by-step in Appendix A (see $(A.5) - (A.12)$).

We find that the PDF of X is given by

$$f_X(x) = \frac{e^{-\frac{x}{\bar{\gamma}_x}}}{2\sqrt{x\bar{\gamma}_x}}\left[-\sqrt{\pi}\,\mathrm{erf}\Big(\sqrt{\frac{x}{\bar{\gamma}_x}}\Big) + 2\sqrt{\frac{x}{\bar{\gamma}_x}}e^{-\frac{x}{\bar{\gamma}_x}} + \frac{2x\sqrt{\pi}}{\bar{\gamma}_x}\mathrm{erf}\Big(\sqrt{\frac{x}{\bar{\gamma}_x}}\Big)\right], \tag{5.8}$$

where $\mathrm{erf}(x) = \frac{2}{\sqrt{\pi}}\int_0^x e^{-t^2}dt$ denotes the error function.

The CDF is given by integration of (5.8):

$$F_X(x) = -\sqrt{\pi}\sqrt{\frac{x}{\bar{\gamma}_x}}e^{-\frac{x}{\bar{\gamma}_x}}\mathrm{erf}\Big(\sqrt{\frac{x}{\bar{\gamma}_x}}\Big) - e^{-\frac{2x}{\bar{\gamma}_x}} + 1. \tag{5.9}$$

5.3 Probability Distribution for Interfering Signal

Following the same procedure as for X, we present the PDF of

$$Y = \bar{\gamma}_y |\mathbf{h_y} \cdot \check{\mathbf{w}}_\mathbf{y}|_{min}^2 = \frac{\bar{\gamma}_y}{2}(|\mathrm{h_{y1}}| - |\mathrm{h_{y2}}|)^2, \tag{5.10}$$

which is the squared difference of two Rayleigh variables, scaled by a constant factor. The PDF is given by

$$f_Y(y) = \frac{e^{-\frac{y}{\bar{\gamma}_y}}}{2\sqrt{y\bar{\gamma}_y}}\left[\sqrt{\pi}\mathrm{erfc}\left(\sqrt{\frac{y}{\bar{\gamma}_y}}\right) + 2\sqrt{\frac{y}{\bar{\gamma}_y}}e^{-\frac{y}{\bar{\gamma}_y}} - \frac{2y\sqrt{\pi}}{\bar{\gamma}_y}\mathrm{erfc}\left(\sqrt{\frac{y}{\bar{\gamma}_y}}\right)\right], \tag{5.11}$$

where $\mathrm{erfc}(y) = 1 - \mathrm{erf}(y)$ denotes the complementary error function.

5.4 Cumulative Distribution Function of SINR

In the previous sections, we presented the exact distributions of X and Y. The CDF of $Z = \frac{X}{1+Y}$ (i.e. the CDF of the RV representing the received SINR at the MUE) can be calculated from the following integral:

$$F_Z(z) = \int_1^\infty F_X(zt)f_Y(t-1)dt, \tag{5.12}$$

where $F_X(x)$ is the CDF of X and $f_Y(y)$ is the PDF of Y. Specifically,

$$F_X(zt) = -\sqrt{\pi}\sqrt{\frac{zt}{\bar{\gamma}_x}}e^{-\frac{zt}{\bar{\gamma}_x}}\mathrm{erf}\left(\sqrt{\frac{zt}{\bar{\gamma}_x}}\right) - e^{-\frac{2zt}{\bar{\gamma}_x}} + 1, \tag{5.13}$$

$$f_Y(t-1) = \frac{e^{-\frac{t-1}{\bar{\gamma}_y}}}{2\sqrt{\bar{\gamma}_y(t-1)}}\left[\sqrt{\pi} - \sqrt{\pi}\mathrm{erf}\left(\sqrt{\frac{t-1}{\bar{\gamma}_y}}\right) + 2\sqrt{\frac{t-1}{\bar{\gamma}_y}}e^{-\frac{t-1}{\bar{\gamma}_y}} - \right.$$
$$\left. \frac{2(t-1)\sqrt{\pi}}{\bar{\gamma}_y} + \frac{2(t-1)\sqrt{\pi}}{\bar{\gamma}_y}\mathrm{erf}\left(\sqrt{\frac{t-1}{\bar{\gamma}_y}}\right)\right]. \tag{5.14}$$

Equation (5.12) includes the product of (5.13) and (5.14), which results to a sum of fifteen different terms. Thus, fifteen integrals need to be calculated and added for derivation of $F_Z(z)$. The exact integrals are presented in Appendix B (see $(B.1) - (B.15)$), along with their respective solutions (see $(B.17) - (B.31)$), which

have been derived after tedious calculations. The final formula for $F_Z(z)$ is the sum of all computed integrals:

$$F_Z(z) = 1 - A_1(z) + \sqrt{\pi} e^{-(\frac{a_z b_z}{2} + \frac{1}{\bar{\gamma}_y})}(A_2(z) - A_3(z)) - 2e^{-2b_z}A_4(z) +$$

$$2e^{-(\frac{a_z b_z}{2} + \frac{1}{\bar{\gamma}_y})}(A_5(z) - A_6(z)), \qquad (5.15)$$

where

$$a_z = 1 + \frac{\bar{\gamma}_x}{z\bar{\gamma}_y}, \ \ b_z = \frac{z}{\bar{\gamma}_x}, \ \ c_z = \frac{\bar{\gamma}_x}{z\bar{\gamma}_y}, \ \ k_i = \frac{(-1)^i}{i!(2i+1)},$$

$$A_1(z) = \frac{2e^{-2b_z}\tan^{-1}\left(\sqrt{1 + \frac{2}{c_z}}\right)}{c_z(1 + \frac{2}{c_z})^{\frac{3}{2}}} + \frac{e^{-2b_z}}{(1 + \frac{2}{c_z})},$$

$$A_2(z) = \sum_{n=0}^{\infty} k_n 2\Gamma\left(\frac{3}{2}\right) a_z^{-\frac{n+7}{2}} b_z^{\frac{n+3}{2}} c_z^{\frac{3}{2}} \ W_{\frac{n+1}{2}, \frac{-n-5}{2}}\left(a_z b_z\right),$$

$$A_3(z) = \sum_{n=0}^{\infty} k_n \Gamma\left(\frac{1}{2}\right) a_z^{-\frac{n+5}{2}} b_z^{\frac{n+1}{2}} c_z^{\frac{1}{2}} \ W_{\frac{n+3}{2}, \frac{-n-3}{2}}\left(a_z b_z\right),$$

$$A_4(z) = \sum_{n=0}^{\infty} \sum_{m=0}^{n+1} \frac{k_n \ (n+1)! \ b_z^m \ c_z}{m! \ (1 + 2c_z)^{n-m+2}},$$

$$A_5(z) = \sum_{n=0}^{\infty} \sum_{m=0}^{\infty} k_n k_m \Gamma(m+1) a_z^{-\frac{m+n+3}{2}} b_z^{\frac{m+n+1}{2}} c_z^{m+1} \ W_{\frac{n-m+1}{2}, \frac{-n-m-2}{2}}\left(a_z b_z\right),$$

$$A_6(z) = \sum_{n=0}^{\infty} \sum_{m=0}^{\infty} k_n k_m 2\Gamma(m+2) a_z^{-\frac{m+n+4}{2}} b_z^{\frac{m+n+2}{2}} c_z^{m+2} \ W_{\frac{n-m}{2}, \frac{-n-m-3}{2}}\left(a_z b_z\right).$$

The results contain the Whittaker function $W_{\lambda,\mu}(x)$, which is a standard form of a confluent hypergeometric function and one of the two solutions of Whittaker's equation [71]. It is evident that the exact outage probability formula for perfect phase feedback involves cumbersome operations. The final formula requires computations of nested infinite sums, some of which need numerous iterations to converge accurately, especially at low SINR values. Despite its non-friendly nature, the resulting theoretical formula proves useful, since it is an illustration of the best possible performance improvement under g-mode 1 and serves as a measure against practical low-rate applications of g-mode 1.

For the scenario presented in Fig. 5.2, there are 17 interferer FBSs, of which the closest one is the dominant interferer. For this case, using the proposed parameters of Table 4.1 (see Chapter 4), the total mean interference plus noise power perceived by the MUE is -64.08 dBm. The MBS is placed at 117.13 meters
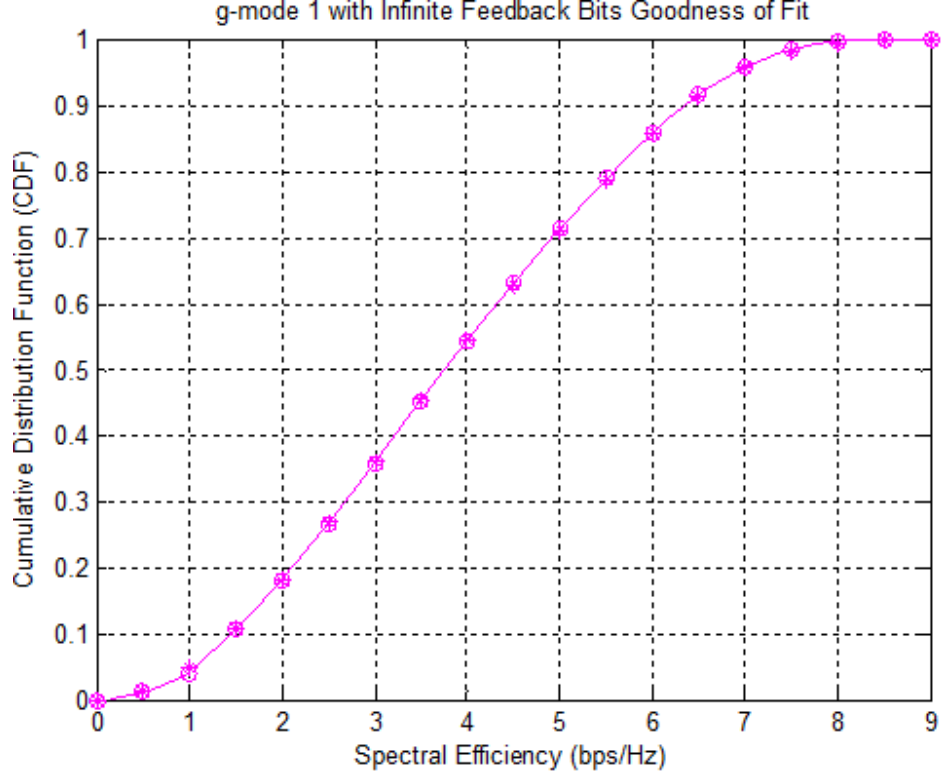
Figure 5.3: Goodness of fit for the CDF of the upper bound SINR perceived by the MUE. Theoretical upper bound is denoted by solid curve (-) and circles (∘), while simulations are denoted by stars (∗).

away from the MUE, so that the received wanted signal is also -64.08 dBm after distance dependent pathloss and penetration loss of an outer and two inner walls. Simulations dictate that the mean SNRs at the MUE in the case of one dominant interferer are $\gamma_{m,1dom} = 17.40$ dB and $\gamma_{1,1dom} = 17.32$ dB, from the MBS and the dominant interferer, respectively.

The goodness of fit for the rate outage probability of the MUE when compared to simulations is shown in Fig. 5.3. In Fig. 5.4 we present simulations of g-mode 1 with $N_p = 1$, $N_p = 2$, $N_p = 3$ phase bits and compare their performance against the theoretical upper bound. It can be seen that even for 3 bits of phase feedback, performance is already close to the upper bound corresponding to perfect phase feedback. Therefore, it is practically achievable to reach performance close to the upper bound with feedback messages of minimal size, and there is no necessity to invest in high-rate feedback links when applying g-mode 1, since the rate gains would be insignificant.
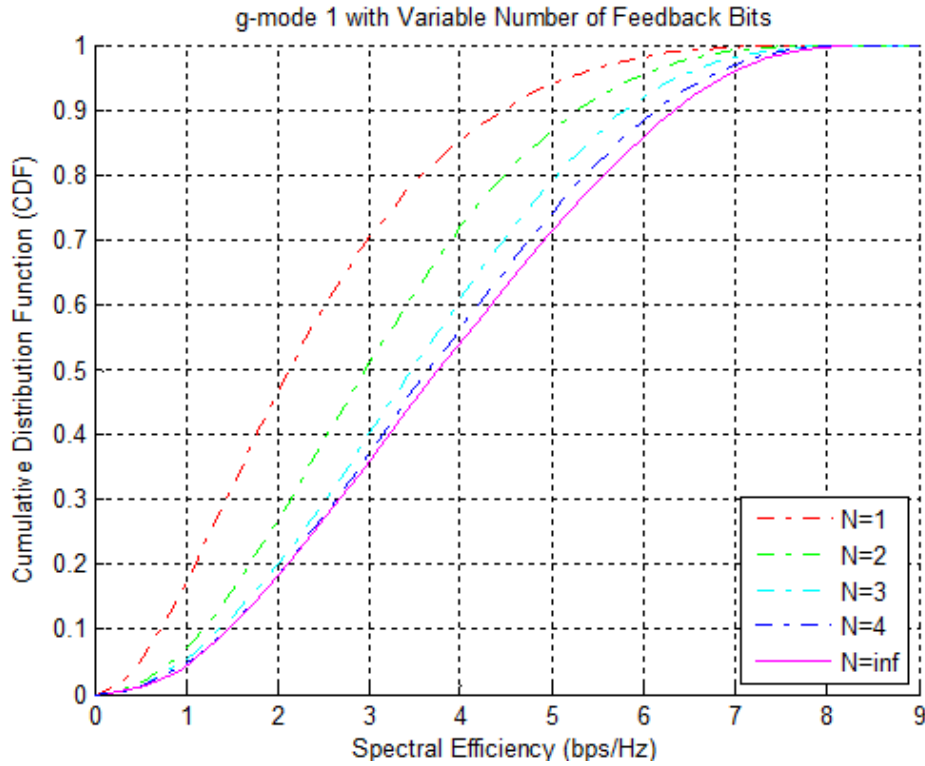
Figure 5.4: Comparison between practical low-rate realizations of g-mode 1 against the optimum upper bound. Theoretical upper bound is denoted by solid curve (-), while simulations are denoted by dashed curves (--). It can be seen that even with feedback message having size as low as 4 bits (blue dashed curve), performance is already very close to the upper bound which would require infinite number of bits.

Chapter 6

Altruistic Beamforming in Multiple Interference Sources

In this section we investigate the SINR and rate outage probability of the MUE as a function of the number of altruistic interferers. We consider that 24 FBSs are transmitting simultaneously in all apartments except the central one, in which the MUE operates (Fig. 6.1). Initially, all FBSs behave egoistically by applying TSC, g-mode 1 or g-mode 2. One-by-one, the interferers apply altruistic TBF, starting from the strongest interferer and gradually reaching the weakest. As shown in section 4.4, the SINR of the MUE in the presence of multiple altruistic interferer FBSs can be modeled as $Z = \frac{X}{1 + \sum\limits_{i \in \mathcal{S}_A} Y_i}$, where $\mathcal{S}_A$ denotes the ordered set of altruistic FBSs according to received power at the MUE, $X = \bar{\gamma}_m |\mathbf{h_m} \cdot \hat{\mathbf{w}}_\mathbf{m}|^2$ represents the desired MBS signal, and $Y_i = \bar{\gamma}_{f_i} |\mathbf{h}_{\mathbf{f_i}} \cdot \check{\mathbf{w}}_{\mathbf{f_i}}|^2$ represents the interference signal from altruistic FBS i.

6.1 Chi-squared Approximations for Desired and Interference Signals

Since exact distributions of the individual RVs (i.e. X and Y_i) are generally difficult to find, we will use those χ^2 approximations presented in [72]. Thus, X can be approximated as a χ^2 RV with 4 degrees of freedom, while each interferer
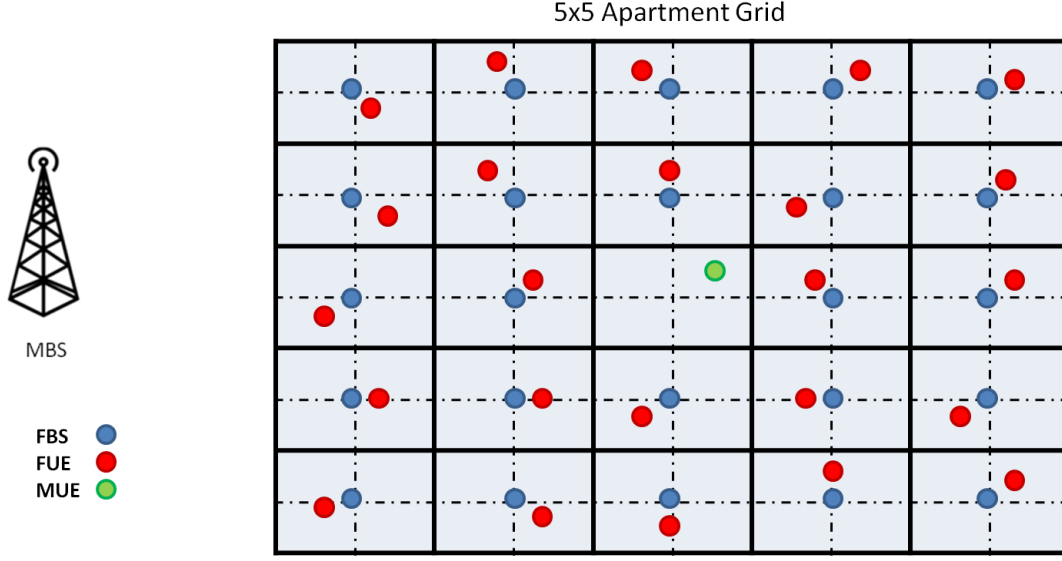
Figure 6.1: The system model comprises of a single MBS-MUE pair and 24 FBS-FUE pairs. The FBSs are located inside a 5-by-5 apartment grid, at the center of apartments (blue dots). All FUEs are randomly placed and experience very good channel conditions from their serving FBS (red dots). The MUE is located in the central apartment (green dot), where no FBS is available.

Y_i can be approximated as an exponential RV. More specifically,

$$F_X(x) = 1 - \left(1 + \frac{2x}{\mathcal{G}\,\bar{\gamma}_m}\right) e^{-\frac{2x}{\mathcal{G}\,\bar{\gamma}_m}} \quad x \geq 0, \tag{6.1}$$

$$f_{Y_i}(y) = \frac{1}{g_i\,\bar{\gamma}_{f_i}} e^{-\frac{y}{g_i\,\bar{\gamma}_{f_i}}} \qquad y \geq 0, \tag{6.2}$$

with $\mathcal{G} = \mathbb{E}\{|\mathbf{h_m} \cdot \hat{\mathbf{w}}_{\mathbf{m}}|^2\}$ and $g_i = \mathbb{E}\{|\mathbf{h_{f_i}} \cdot \check{\mathbf{w}}_{\mathbf{f_i}}|^2\}$ denoting the beamforming gains from egoistic and altruistic TBF, respectively. In case of TSC, expectations $\mathcal{G}$ and g_i (for $i \in \mathcal{S}_A$) admit values equal to:

$$\mathcal{G} = \frac{3}{2}, \; g_i = \frac{1}{2}. \tag{6.3}$$

In case of g-mode 1 and g-mode 2, expectations $\mathcal{G}$ and g_i (for $i \in \mathcal{S}_A$) depend on the number of phase bits N included in the feedback message. Closed-form expressions for egoistic and altruistic beamforming gains were derived in [72]. Specifically, for g-mode 1,

$$\mathcal{G} = 1 + \frac{\pi}{4}a_N, \; g_i = 1 - \frac{\pi}{4}a_N, \; a_N = \frac{2^N}{\pi}\sin\left(\frac{\pi}{2^N}\right). \tag{6.4}$$

Similarly, for g-mode 2,

$$\mathcal{G} = 1 + \frac{\pi}{4}\sqrt{\frac{4}{\pi^2} + a_N^2}, \ \mathrm{g}_i = 1 - \frac{\pi}{4}\sqrt{\frac{4}{\pi^2} + a_N^2}. \tag{6.5}$$

6.2 Egoistic TBF in all FBS Interferers

For the case of $|\mathcal{S}_A| = 0$, where all FBS interferers apply egoistic beamforming, the received SINR at the MUE follows a χ^2 distribution with signals from all egoistic interferers considered as background noise. Then, the outage probability for the received SINR at the MUE is given by:

$$F_{Z_{\mathrm{mue}}^{(0)}}(z) = 1 - \left(1 + \frac{2z}{\mathcal{G}\bar{\gamma}_m}\right)e^{-\frac{2z}{\mathcal{G}\bar{\gamma}_m}} \qquad z \geq 0, \tag{6.6}$$

where $Z_{\mathrm{mue}}^{(0)}$ denotes the SINR at the MUE with 0 dominant altruistic interferers, and $\bar{\gamma}_m \equiv \bar{\gamma}_{m,|\mathcal{S}_A|=0}$.

6.3 Altruistic TBF only in Dominant FBS Interferer

For the case of $|\mathcal{S}_A| = 1$, where only one dominant FBS altruistic interferer is considered, closed-form expressions for the SINR distribution of the victim MUE have been presented in [73]. That work focused on co-layer interference, but results directly apply to cross-layer interference scenarios, where the assumption of a single dominant interferer is justified. The SINR outage probability for the MUE user in case of a single dominant interferer is then given by

$$F_{Z_{\mathrm{mue}}^{(1)}}(z) = 1 - e^{-\frac{2z}{\mathcal{G}\bar{\gamma}_m}}\left[\frac{\frac{2z\,\mathcal{G}\,\bar{\gamma}_m}{\mathrm{g}_1\,\bar{\gamma}_{f_1}}}{\left(\frac{\mathcal{G}\,\bar{\gamma}_m}{\mathrm{g}_1\,\bar{\gamma}_{f_1}} + 2z\right)^2} + \frac{\left(1 + \frac{2z}{\mathcal{G}\,\bar{\gamma}_m}\right)\frac{\mathcal{G}\,\bar{\gamma}_m}{\mathrm{g}_1\,\bar{\gamma}_{f_1}}}{\frac{\mathcal{G}\,\bar{\gamma}_m}{\mathrm{g}_1\,\bar{\gamma}_{f_1}} + 2z}\right] \qquad z \geq 0, \tag{6.7}$$

where $\bar{\gamma}_m \equiv \bar{\gamma}_{m,|\mathcal{S}_A|=1}$, $\bar{\gamma}_{f_1} \equiv \bar{\gamma}_{f_1,|\mathcal{S}_A|=1}$.

6.4 Altruistic TBF in Multiple Dominant FBS Interferers

In this section we assume that at least two FBS interferers apply altruistic TBF. More specifically, we investigate two cases, in which:

1. the mean received interference powers from different FBSs are different,

2. the mean received interference powers are equal. The former corresponds
   to most practical real-life scenarios, while the latter represents a specific
   case study with primarily theoretical value.

6.4.1 Multiple Interferers with Different Mean Received Powers at the MUE

For cases with $|\mathcal{S}_A| = \ell$, with $\ell \geq 2$, we first derive the PDF of the sum $\sum_{i \in \mathcal{S}_A} Y_i$ of exponential RVs present in the denominator of (4.3). This requires repeated usage of convolution, between the distributions of the interferers. For $|\mathcal{S}_A| = 2$, we find that

$$f_Y(y) = \begin{cases} \dfrac{y e^{-\frac{y}{g_1 \bar{\gamma}_{f_1}}}}{g_1^2 \bar{\gamma}_{f_1}^2}, & \text{if } g_1 \bar{\gamma}_{f_1} = g_2 \bar{\gamma}_{f_2}, \\[3ex] \dfrac{e^{-\frac{y}{g_2 \bar{\gamma}_{f_2}}} - e^{-\frac{y}{g_1 \bar{\gamma}_{f_1}}}}{g_2 \bar{\gamma}_{f_2} - g_1 \bar{\gamma}_{f_1}} & \text{otherwise,} \end{cases} \tag{6.8}$$

with $y \geq 0$, $\bar{\gamma}_m \equiv \bar{\gamma}_{m,|\mathcal{S}_A|=2}$, $\bar{\gamma}_{f_i} \equiv \bar{\gamma}_{f_i,|\mathcal{S}_A|=2}$ for i=1,2.

For the derivation of the generalized PDF, we assume that mean received powers from different transmitters differ at least slightly (i.e. $g_i \bar{\gamma}_{f_i} \neq g_j \bar{\gamma}_{f_j}$, $\forall i \neq j$). This assumption, which applies to most practical scenarios, allows us to focus on one branch of the convolution, at each stage. Then, successive convolutions yield a pattern in the PDF derivation, which is given by the following closed-form formula for $|\mathcal{S}_A| \geq 2$:

$$f_Y(y) = \left[\prod_{i \in \mathcal{S}_A} \frac{1}{g_i \bar{\gamma}_{f_i}} \right] \sum_{j \in \mathcal{S}_A} \frac{e^{-\frac{y}{g_j \bar{\gamma}_{f_j}}}}{\prod_{\substack{k \neq j \\ k \in \mathcal{S}_A}} \left(\frac{1}{g_k \bar{\gamma}_{f_k}} - \frac{1}{g_j \bar{\gamma}_{f_j}} \right)} \quad y \geq 0. \tag{6.9}$$

For details on the derivation of the above formula, see [74]. The CDF of Z can then be calculated by substituting (6.1) and (6.9) into the following formula [75]:

$$F_Z(z) = \int_1^\infty F_X(zt) f_Y(t-1) dt. \tag{6.10}$$

After manipulations, the CDF of Z for $|\mathcal{S}_A| = \ell$, with $\ell \geq 2$ is found to be

$$F_{Z_{\text{mue}}^{(\ell)}}(z) = \left[\prod_{i \in \mathcal{S}_A} \frac{1}{g_i \, \bar{\gamma}_{f_i}} \right] \times$$

$$\sum_{j \in \mathcal{S}_A} \frac{g_j \, \bar{\gamma}_{f_j} - e^{-\frac{2z}{\mathcal{G} \, \bar{\gamma}_m}} \left(\frac{1 + \frac{\mathcal{G} \, \bar{\gamma}_m}{2z}}{1 + \frac{\mathcal{G} \, \bar{\gamma}_m}{2z g_j \, \bar{\gamma}_{f_j}}} + \frac{\frac{\mathcal{G} \, \bar{\gamma}_m}{2z}}{(1 + \frac{\mathcal{G} \, \bar{\gamma}_m}{2z g_j \, \bar{\gamma}_{f_j}})^2} \right)}{\prod_{\substack{k \neq j \\ k \in \mathcal{S}_A}} \left(\frac{1}{g_k \, \bar{\gamma}_{f_k}} - \frac{1}{g_j \, \bar{\gamma}_{f_j}} \right)} \quad z \geq 0, \qquad (6.11)$$

where $\bar{\gamma}_m \equiv \bar{\gamma}_{m,|\mathcal{S}_A|=\ell}$, $\bar{\gamma}_{f_i} \equiv \bar{\gamma}_{f_i,|\mathcal{S}_A|=\ell}$ for $i = 1, 2, ..., \ell$.

For illustrating the results, we assume that the MBS applies egoistic g-mode 1 with length of feedback message equal to 2 bits. Figures 6.2-6.6 illustrate the outage capacity distribution for the MUE, when a variable number of FBS interferers apply altruistic TBF using TSC, g-mode 1 with 2 and 3 phase feedback bits, and g-mode 2 with a total of 3 and 4 feedback bits (i.e. 1 bit for amplitude and the rest for phase). In general, it can be observed that theoretical and simulation results match very well. Slight deviations, that do not affect results significantly, can be seen in the cases of g-mode 1 with 3 bits and g-mode 2 with 4 bits, which result from the nature of the approximations used. Nevertheless, accurate results are guaranteed for up to the 50th-percentile value.

For all modes, as the number of altruistic interferers increases, performance gains can be observed until saturation is reached at the upper bound. The performance difference between the purely egoistic (red curve) and the purely altruistic case (black curve) is smallest in the case of TSC; thus, only few interferers need to be considered but the improvements in outage capacity are not dramatic. The best performance achieved by TSC for the 50th-percentile outage capacity is approximately equal to 2 bps/Hz, which denotes an almost 67 % improvement over the egoistic case of 1.2 bps/Hz. Usage of g-mode 1 with 2 bits provides better results than TSC and can increase the 50th-percentile rate of the MUE to a value of about 2.8 bps/Hz with the usage of one more feedback bit. By adding one more bit (i.e. total of 3 bits), g-mode 1 continues to improve performance (i.e. 50th-percentile reaches 3 bps/Hz) but the improvement is less noticeable. It is clear that g-mode 2 provides the best potential for MUE performance gains, with a possible 4.2 bps/Hz value for the 50th-percentile outage capacity, corresponding to an improvement of around 250% compared to the egoistic case.
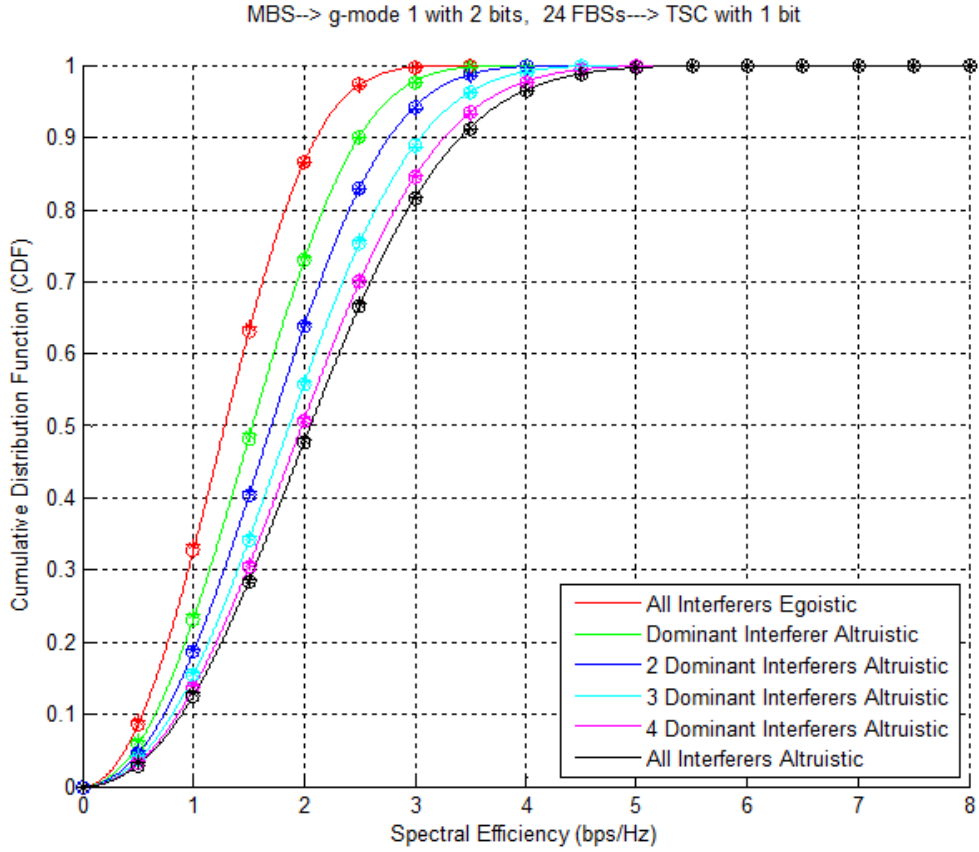
Figure 6.2: MUE outage capacity when a variable number of interferers apply altruistic TSC. Solid lines (-) and circles (○) depict the CDF which was derived analytically, while stars (∗) mark the empirical CDF, obtained through simulations. Red line depicts the case when all FBSs apply egoistic TBF. Green, blue, cyan and magenta lines correspond to cases where one, two, three and four dominant interferer FBSs apply altruistic TBF, respectively. Black line depicts the case where all interferer FBSs apply altruistic TBF.
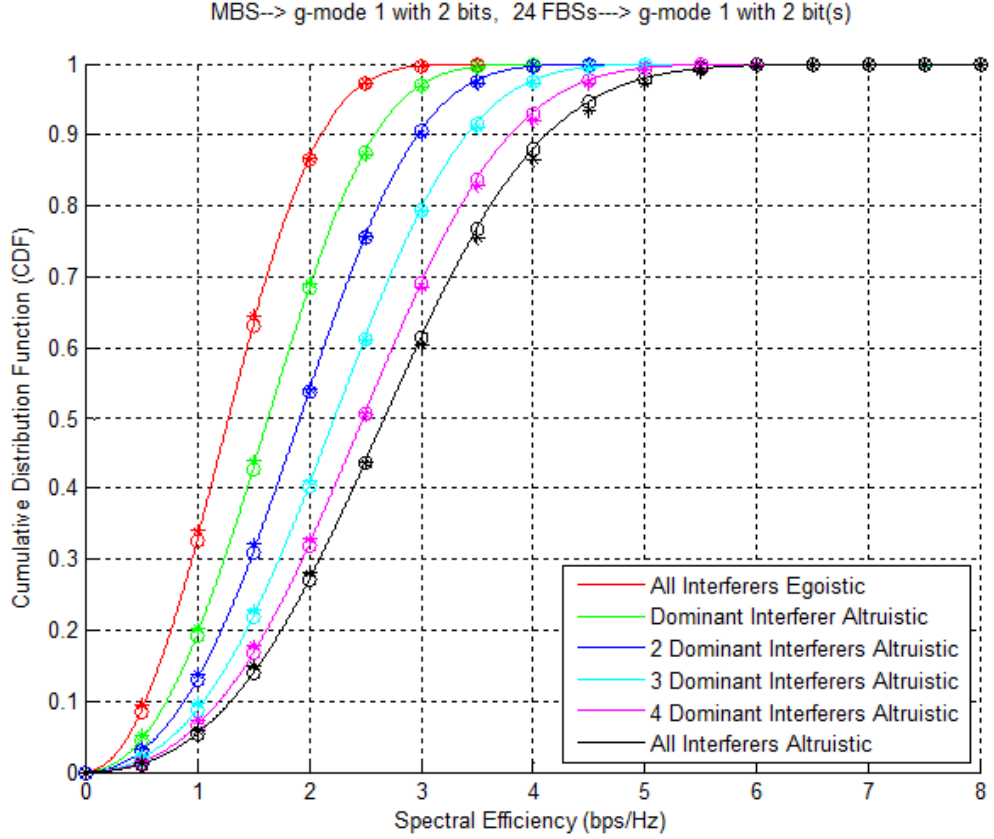
Figure 6.3: MUE outage capacity when a variable number of interferers apply altruistic g-mode 1 with 2 bits. Solid lines (-) and circles (∘) depict the CDF which was derived analytically, while stars (∗) mark the empirical CDF, obtained through simulations. Red line depicts the case when all FBSs apply egoistic TBF. Green, blue, cyan and magenta lines correspond to cases where one, two, three and four dominant interferer FBSs apply altruistic TBF, respectively. Black line depicts the case where all interferer FBSs apply altruistic TBF.
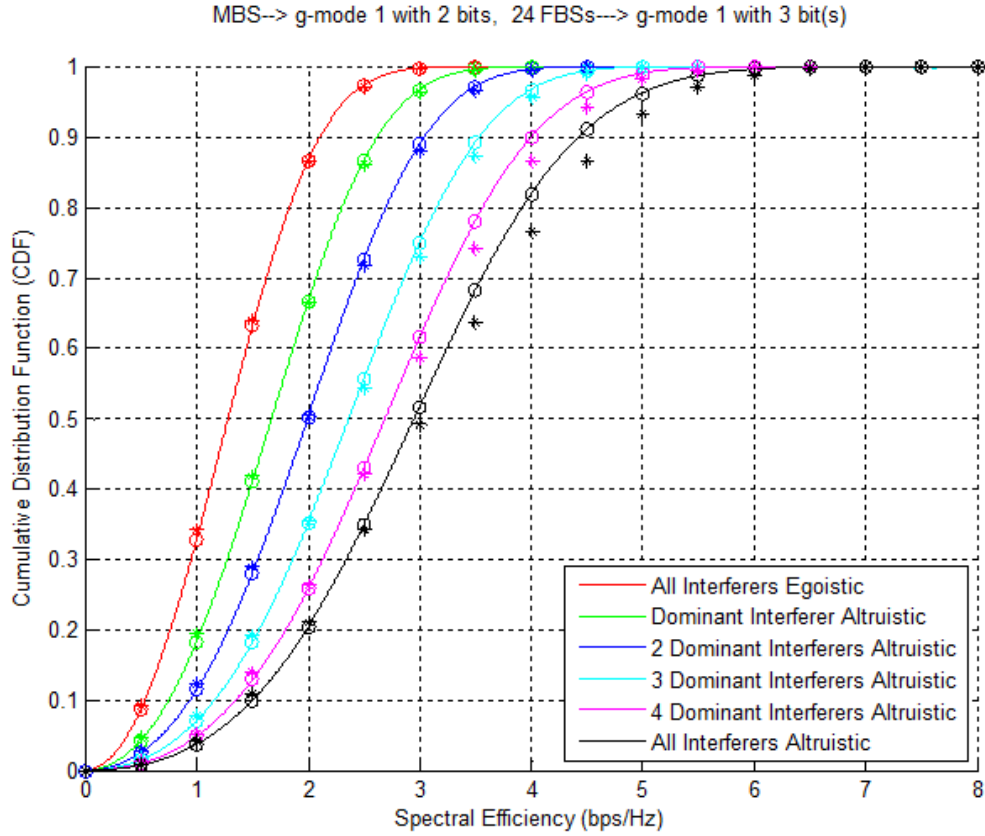
Figure 6.4: MUE outage capacity when a variable number of interferers apply altruistic g-mode 1 with 3 bits. Solid lines (-) and circles (○) depict the CDF which was derived analytically, while stars (∗) mark the empirical CDF, obtained through simulations. Red line depicts the case when all FBSs apply egoistic TBF. Green, blue, cyan and magenta lines correspond to cases where one, two, three and four dominant interferer FBSs apply altruistic TBF, respectively. Black line depicts the case where all interferer FBSs apply altruistic TBF.
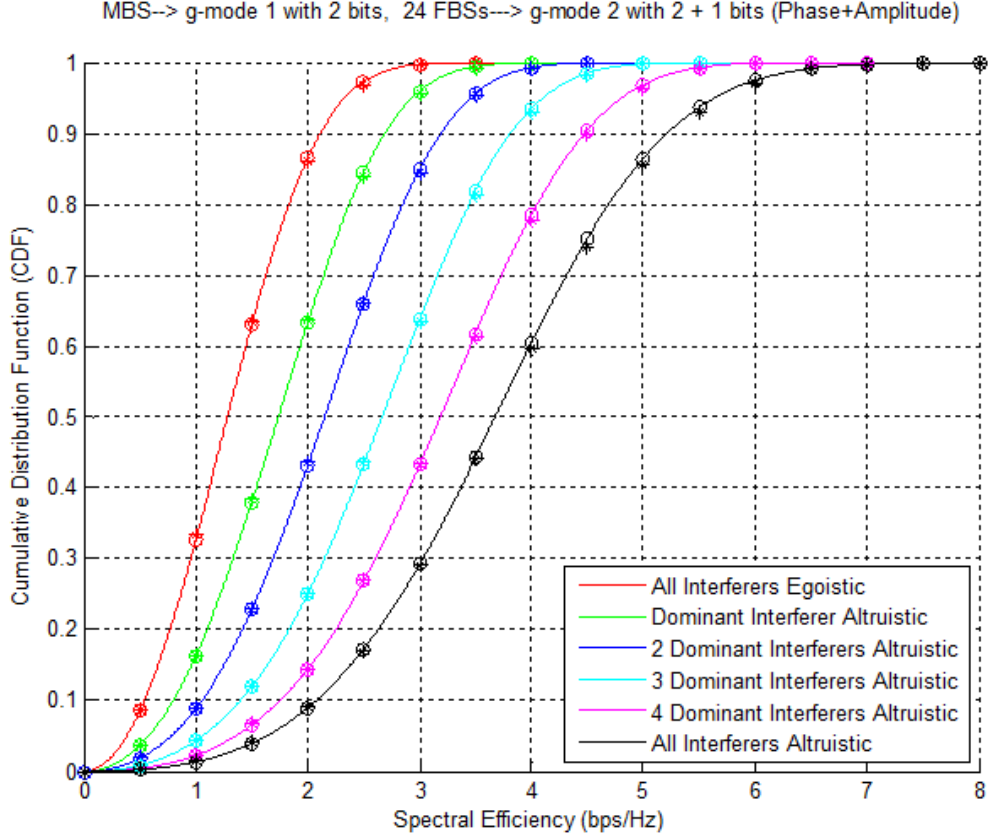
Figure 6.5: MUE outage capacity when a variable number of interferers apply altruistic g-mode 2 with 3 bits (i.e. 2 phase bits and 1 amplitude bit with optimal amplitude weights). Solid lines (-) and circles (○) depict the CDF which was derived analytically, while stars (∗) mark the empirical CDF, obtained through simulations. Red line depicts the case when all FBSs apply egoistic TBF. Green, blue, cyan and magenta lines correspond to cases where one, two, three and four dominant interferer FBSs apply altruistic TBF, respectively. Black line depicts the case where all interferer FBSs apply altruistic TBF.
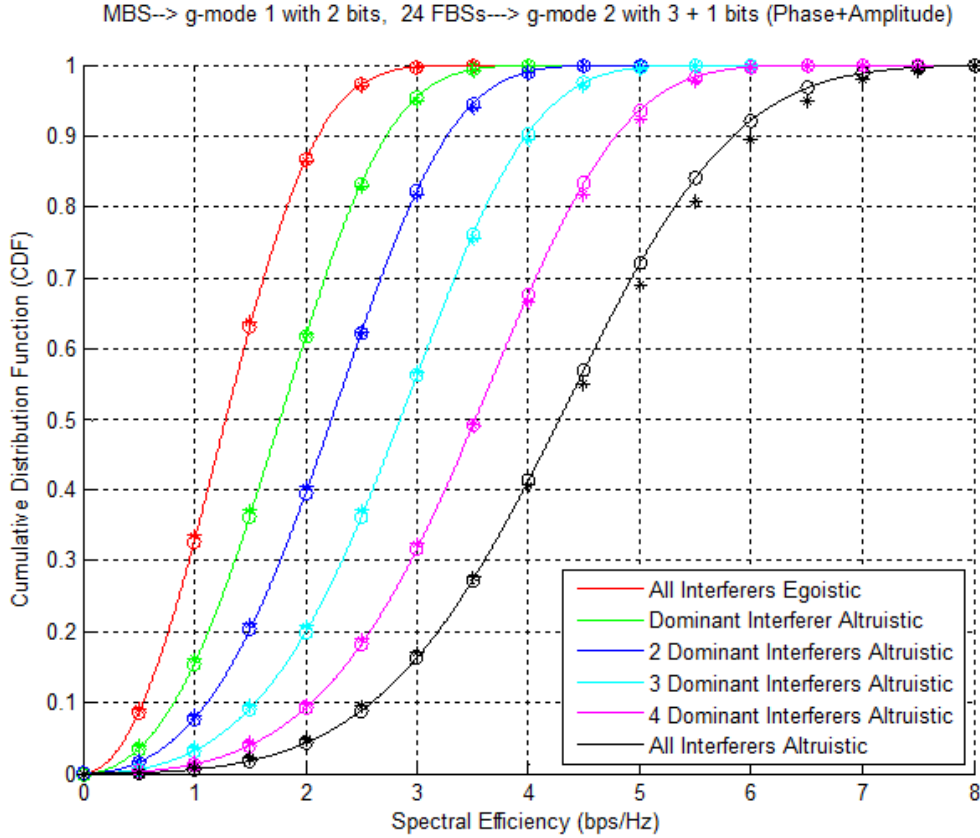
Figure 6.6: MUE outage capacity when a variable number of interferers apply altruistic g-mode 2 with 4 bits (i.e. 3 phase bits and 1 amplitude bit with optimal amplitude weights). Solid lines (-) and circles (∘) depict the CDF which was derived analytically, while stars (∗) mark the empirical CDF, obtained through simulations. Red line depicts the case when all FBSs apply egoistic TBF. Green, blue, cyan and magenta lines correspond to cases where one, two, three and four dominant interferer FBSs apply altruistic TBF, respectively. Black line depicts the case where all interferer FBSs apply altruistic TBF.

The 10th and 50th percentile spectral efficiency values are illustrated in figures 6.7 and 6.8 respectively. Curves for complete CSIT and complete phase CSIT have also been included for comparison. It is evident that mitigation of more than 12 interferers provides almost no gain for the MUE, independent of the mode used. Thus, there is no need to sacrifice the beamforming gain of any of the 12 weakest interferers. Most importantly, it can be observed that curves have almost constant slope for certain groups of altruistic interferers. This observation yields that application of altruistic TBF provides best gains when it is performed in *clusters*, taking advantage of the system topology. For the specific system presented in Fig. 6.1, it is best to consider clusters of four interferers. The first cluster consists of the four dominant interferers and the remaining clusters are defined in a similar way, according to their level of mean interference power towards the MUE.

Consider the 10th-percentile outage capacity of Fig. 6.7. For the TSC case, mitigation of the first cluster is enough for reaching the performance upper bound. For g-mode 1, mitigation of at most two clusters is sufficient for reaching the upper bound. Indeed, even for infinite number of available phase feedback bits, considering more clusters provides no gain in performance. Algorithm g-mode 2 with 4 bits is the only method of those with limited feedback that still provides noticeable gains in the 10th-percentile outage capacity when considering a third cluster. In general, the above observations also apply for the 50th- percentile outage capacity (see Fig. 6.8), even though there can be observed slight improvements when considering a second cluster for TSC or a third cluster for g-mode 1. From the above observations, it is clear that the optimal number of participating clusters depends on the mode used and the chosen resolution for the feedback message.
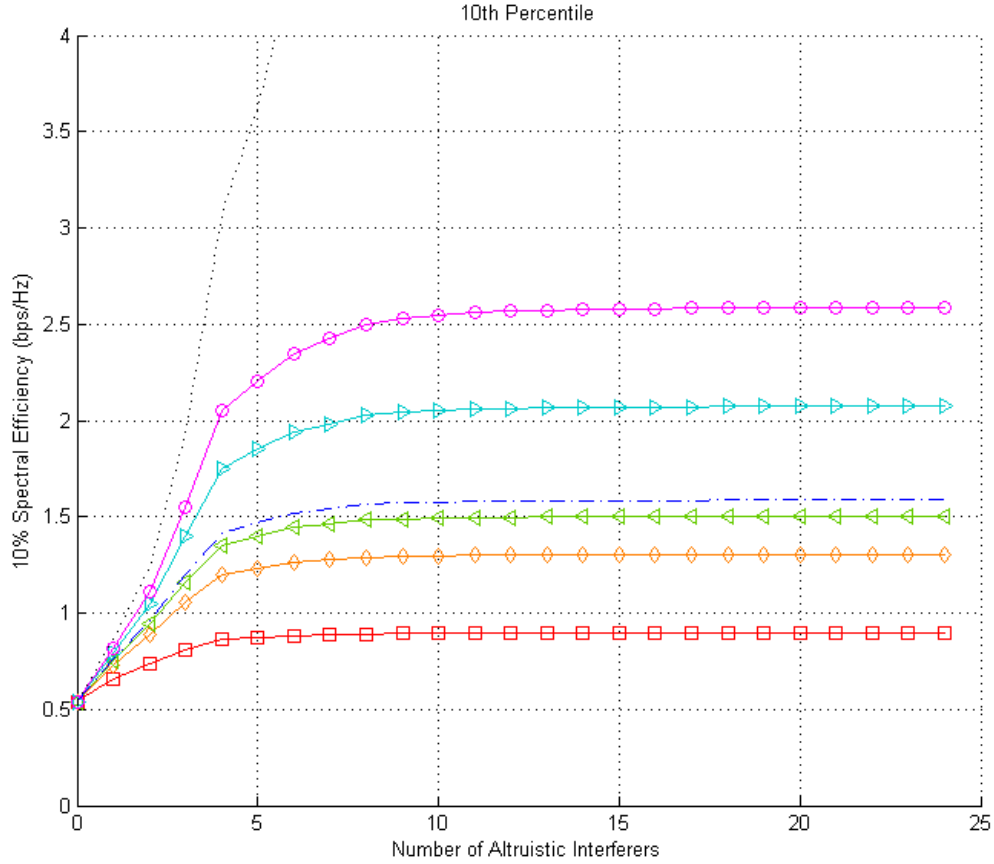
Figure 6.7: Theoretically derived 10th-percentile MUE outage capacity with respect to number
of altruistic FBS interferers. Red squared line (□) represents TSC. Orange diamond line (◇)
denotes g-mode 1 with 2 bits, while green left-pointing triangle line (◁) denotes g-mode 1 with
3 bits. The blue dotted line (.-) represents g-mode 1 with infinite feedback resolution. Cyan
right-pointing triangle line (▷) represents g-mode 2 with 3 bits, while magenta circled line (○)
depicts g-mode 2 with 4 bits. The black dotted line (.) represents complete cancellation of
interferers.
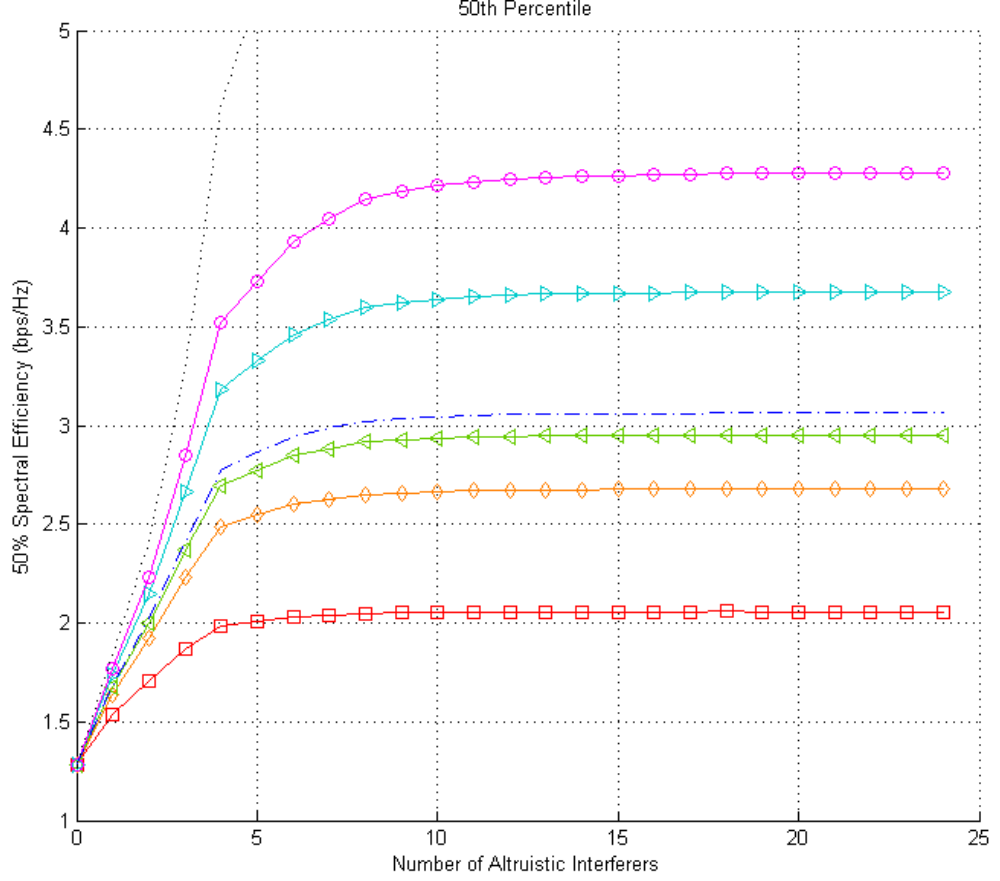
Figure 6.8: Theoretically derived 50th-percentile MUE outage capacity with respect to number of altruistic FBS interferers. Red squared line ($\square$) represents TSC. Orange diamond line ($\diamond$) denotes g-mode 1 with 2 bits, while green left-pointing triangle line ($\triangleleft$) denotes g-mode 1 with 3 bits. The blue dotted line (.-) represents g-mode 1 with infinite feedback resolution. Cyan right-pointing triangle line ($\triangleright$) represents g-mode 2 with 3 bits, while magenta circled line ($\circ$) depicts g-mode 2 with 4 bits. The black dotted line (.) represents complete cancellation of interferers.

6.4.2 Multiple Interferers with Equal Received Powers at the MUE

In the case that the mean received powers from a sufficiently large number of interferers at the MUE are at the same level, the Central Limit Theorem (CLT) can be applied for approximating the total interference power at the MUE as a Gaussian distribution. More specifically, the PDF of the sum of interference $Y = \sum_{i \in \mathcal{S}_A} Y_i$ is modeled as a truncated Gaussian PDF with mean equal to the sum of the means and variance equal to the sum of the variances of the individual interferers Y_i. For simplicity, we assume that the mean received SNR from each interferer has the same value $\bar{\gamma}$, but the approximation also works well in cases where mean SNRs from the different interferers have small deviations from that value. Truncation is necessary, since each interferer RV represents a non-negative SNR value, thus the sum cannot be negative. Although interferer RVs must be i.i.d., this approach is independent of the actual distribution of each interferer; therefore, it is not restricted to modeling each interferer RV as exponential.

If $|\mathcal{S}_A| = k$ interferers apply a certain altruistic beamforming method with gain g, and the mean received SNR from each interferer to the MUE is $\bar{\gamma}$, the sum of interference can be modeled as a Gaussian RV, symbolized Y_{Gauss}, with PDF given by

$$f_{Y_{Gauss}}(y) = \frac{1}{Q(-\frac{\mu}{\sigma})} \frac{1}{\sqrt{2\pi}\sigma} e^{-\frac{(y-\mu)^2}{2\sigma^2}}, \tag{6.12}$$

where $\mu = \sum_{i=1}^{k}(\text{g}_i \, \bar{\gamma}_i) = k \, \text{g} \, \bar{\gamma}$ is the mean value, $\sigma = \sqrt{\sum_{i=1}^{k}(\text{g}_i^2 \, \bar{\gamma}_i^2)} = \sqrt{k \, \text{g}^2 \, \bar{\gamma}^2}$ is the standard deviation and Q(.) denotes the Q-function given by the formula $Q(x) = \frac{1}{\sqrt{2\pi}} \int_x^{\infty} \exp\left(-\frac{u^2}{2} du\right)$. Considering X as a 4 degree-of-freedom chi-squared RV with mean $\mathcal{G} \, \bar{\gamma}_x$, the RV

$$Z = \frac{X}{1 + \sum\limits_{i \in \mathcal{S}_A} Y_i} = \frac{X}{1 + Y_{Gauss}} \tag{6.13}$$

can be found by substitution of F_X and $f_{Y_{Gauss}}$ into

$$F_Z(z) = \int_1^{\infty} F_X(zt) f_{Y_{Gauss}}(t-1) dt, \tag{6.14}$$

After some manipulations, it can be shown that

$$F_Z(z) = \frac{1}{Q(-\frac{\mu}{\sigma})} \left[\frac{1}{2}\text{erfc}\left(-\frac{\mu}{\sqrt{2}\sigma}\right) - \frac{\sqrt{2}\,\sigma\,z}{\sqrt{\pi}\mathcal{G}\,\bar{\gamma}_m} e^{-\frac{2z}{\mathcal{G}\,\bar{\gamma}_m} - \frac{\mu^2}{2\sigma^2}} - \text{erfc}\left(\frac{\sqrt{2}\,\sigma\,z}{\mathcal{G}\,\bar{\gamma}_m} - \frac{\mu}{\sqrt{2}\sigma}\right) \times \right.$$
$$\left. \exp\left(-\frac{2(\mu+1)z}{\mathcal{G}\,\bar{\gamma}_m} + \frac{2(\sigma\,z)^2}{(\mathcal{G}\,\bar{\gamma}_m)^2}\right) \left(\frac{1}{2} + \frac{(\mu+1)z}{\mathcal{G}\,\bar{\gamma}_m} - \frac{2(\sigma\,z)^2}{(\mathcal{G}\,\bar{\gamma}_m)^2}\right) \right]. \tag{6.15}$$
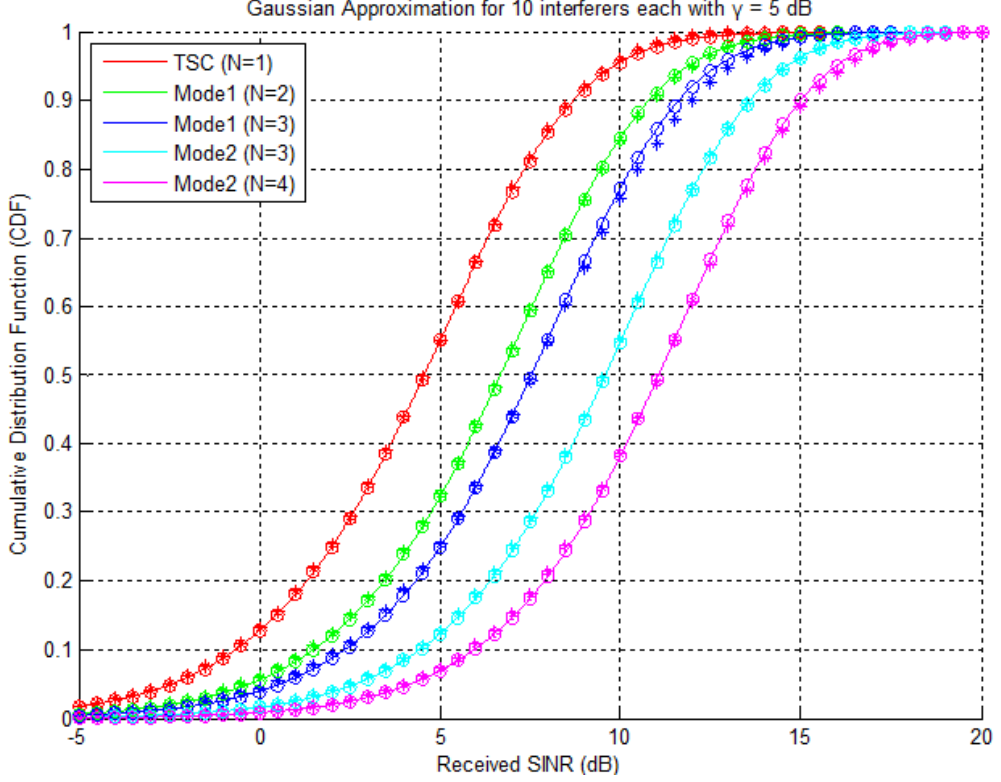
Figure 6.9: SINR of MUE in the case of 10 interferers with received SNR mean value around 5 dB from each. The SNR from MBS is equal to the sum of interference. Gaussian approximation for the sum interference signal power is used. Theoretical curves are denoted by solid curve (-) and circles (○), while simulations are denoted by stars (∗).

Consider a system model of 10 interferer FBSs with transmission powers such that the individual SNR received at the MUE from each interferer is $\bar{\gamma} = 5$ dB. This scenario could be achieved through a ring topology for 10 FBSs with equal transmission powers and an MUE user at the center of the ring. Furthermore, consider that the received SNR from the MBS is $\bar{\gamma}_m = 15.13$ dB such that the mean SINR at the MUE is 0 dB. Suppose that the MBS applies egoistic g-mode 1 with $N_p = 2$ bits and that all interferers apply altruistic g-mode 1 with $N_p = 2$ bits. From Fig. 6.9, we observe that the resulting CDF of the SINR provides an almost perfect match with the simulation values. The resulting gain of commanding 10 interferers to become altruistic can be observed from the improvement in the 50th-percentile SINR value by approximately 7 dB, as shown in Fig. 6.9.

6.5 Performance Degradation at the FUE

So far, we have dealt only with the performance of the MUE. Initially, from the perspective of an FUE served by an egoistic FBS, the SINR follows a χ^2 distribution with 4 degrees of freedom and mean $\mathcal{G}_f \bar{\gamma}_f$, where $\mathcal{G}_f$ is the beamforming gain from the TBF method applied at the FBS, and $\bar{\gamma}_f$ is the mean SINR perceived at the FUE. This is due to the fact that all of its perceived interferers (i.e. the remaining FBSs and the MBS) are treated as background noise, since no cochannel interference mitigation is performed by other BSs towards the particular FUE (i.e. $|\mathcal{S}_{A_f}| = 0$). The CDF of the SINR for the FUE, assuming that its serving FBS is egoistic, is given by

$$F_{Z_{\text{fue}}^{(0)}}(z) = 1 - \left(1 + \frac{2z}{\mathcal{G}\bar{\gamma}_f}\right) e^{-\frac{2z}{\mathcal{G}\bar{\gamma}_f}} \qquad z \geq 0, \qquad (6.16)$$

where $Z_{\text{fue}}^{(0)}$ denotes the SINR at the FUE with 0 dominant altruistic interferers, and $\bar{\gamma}_f \equiv \bar{\gamma}_{f,|\mathcal{S}_{A_f}|=0}$ denotes the respective mean SINR at the FUE.

When the FBS shifts its behavior from egoistic to altruistic, the desired signal X received by its associated FUE becomes exponentially distributed with mean $\bar{\gamma}_f$. Then, the SINR at the FUE follows an exponential distribution:

$$F_{Z_{\text{fue}}^{(0)}}(z) = 1 - e^{-\frac{z}{\bar{\gamma}_f}}, \qquad z \geq 0. \qquad (6.17)$$

Mean loss of performance for each FUE, when its serving FBS applies altruistic TBF, is equal to the beamforming gain $\mathcal{G}$ that is not present anymore. In a high SINR regime, this is usually equivalent to an insignificant loss in achievable data rate.

Chapter 7

Extensions of Altruistic Beamforming Methods

So far, in order to improve performance of an interfered MUE in a HetNet setting, we have used the practical algorithms of TSC, g-mode 1 and g-mode 2 for interference mitigation exactly as found in [66][73] for the two-antenna case. In this chapter, we investigate modifications of these methods to

1. include more precise amplitude feedback, and

2. to work efficiently when transmitters possess more than two transmit antennas.

As an initial study, we will concentrate in adding one more bit for amplitude resolution in the feedback message of g-mode 2. In addition, we will present our multi-antenna interference scheme for the case of 4 antennas, which can easily be generalized for 2^n, where $n \in \mathbb{N}$ represents the number of transmit antennas.

7.1   Increasing Amplitude Feedback Resolution

Although the feedback message of g-mode 2 contains information about the order of channel gain amplitudes, it is clear that primary emphasis has been given on the phase resolution. For the case of two transmit antennas, g-mode 2 dedicates only one bit for the feedback of channel amplitude information. Therefore, the only permitted action regarding amplitude information is feeding back to the transmitter the index corresponding to the strongest/weakest antenna. Consider the case where the amplitudes of the two channel gains are approximately equal.

Then, the receiver must identify and send back to the transmitter the index of the
best antenna (i.e., for interference mitigation, the one with the weakest channel),
without providing information about the strength relationship between antennas.
Thus, considering optimal amplitude weights, approximately 80 % of the power
will be allocated to the slightly better antenna, and only 20 % to the weaker
antenna, although their channel conditions are similar. This example signifies
that knowledge of the relative strength between the two channel gains (i.e., soft
order information) could further improve the performance of g-mode 2.

In this section, we investigate the performance of increased amplitude feedback
resolution for altruistic beamforming, in cases where interferers are equipped
with two transmit antennas. More specifically, we consider that the feedback
message contains two bits dedicated to amplitude information and the remaining
for phase. We define a threshold value for the difference between the amplitudes
of the two channel gains. Then, different amplitude weights are applied when
the instantaneous amplitude difference of the channel gains is higher or lower
than the predefined threshold. By means of a brute force search, we identify the
optimal amplitude weights that should be applied for a given threshold. More
specifically, we vary the threshold value between the two channel gain amplitudes
from 1 to 10 dB in unitary dB steps. Then, for each threshold, brute force
search is performed to find optimal amplitude weights for cases where the channel
amplitude difference is above and below the threshold. The optimal amplitude
weights for a list of threshold values are shown in tables 7.1-7.4, together with
the respective SNR gains perceived by the victim MUE on the interference link
(i.e. the weaker the signal received, the higher the gain for the MUE), against the
case where no beamforming is used and SNR gain is 0 dB. Each amplitude weight
vector contains two amplitude weights, with the first/smallest value applied to
the strongest antenna. In all cases, the optimal threshold values for a fixed-length
feedback message are shown in bold. These are the values that will be chosen for
comparisons against traditional g-mode 2.

Table 7.1: Soft-order g-mode 2 with 1 bit for phase and 2 bits for amplitude. Gains are concentrated around the value of 6 dB, with the best gain equal to 6.1 dB, achieved for threshold equal to 5 dB.

$N_b = 3$ bits	Optimal Amplitude Weights		
Threshold T (dB)	$\|\|h_1(dB)\| - \|h_2(dB)\|\| > T$	$\|\|h_1(dB)\| - \|h_2(dB)\|\| \leq T$	Gain (dB)
1	$[\sqrt{0.1230} \quad \sqrt{0.8770}]$	$[\sqrt{0.4550} \quad \sqrt{0.5450}]$	5.66
2	$[\sqrt{0.1020} \quad \sqrt{0.8980}]$	$[\sqrt{0.4130} \quad \sqrt{0.5870}]$	5.87
3	$[\sqrt{0.0830} \quad \sqrt{0.9170}]$	$[\sqrt{0.3730} \quad \sqrt{0.6270}]$	6.01
4	$[\sqrt{0.0680} \quad \sqrt{0.9320}]$	$[\sqrt{0.3380} \quad \sqrt{0.6620}]$	6.08
5	$[\sqrt{\mathbf{0.0550}} \quad \sqrt{\mathbf{0.9450}}]$	$[\sqrt{\mathbf{0.3060}} \quad \sqrt{\mathbf{0.6940}}]$	**6.10**
6	$[\sqrt{0.0440} \quad \sqrt{0.9560}]$	$[\sqrt{0.2780} \quad \sqrt{0.7220}]$	6.07
7	$[\sqrt{0.0350} \quad \sqrt{0.9650}]$	$[\sqrt{0.2550} \quad \sqrt{0.7450}]$	6.03
8	$[\sqrt{0.0280} \quad \sqrt{0.9720}]$	$[\sqrt{0.2360} \quad \sqrt{0.7640}]$	5.96
9	$[\sqrt{0.0220} \quad \sqrt{0.9780}]$	$[\sqrt{0.2190} \quad \sqrt{0.7810}]$	5.89
10	$[\sqrt{0.0180} \quad \sqrt{0.9820}]$	$[\sqrt{0.2060} \quad \sqrt{0.7940}]$	5.82

Table 7.2: Soft-order g-mode 2 with 2 bits for phase and 2 bits for amplitude. The best gain is 10.74 dB, achieved for threshold equal to 6 dB.

$N_b = 4$ bits	Optimal Amplitude Weights		
Threshold T (dB)	$\|\|h_1(dB)\| - \|h_2(dB)\|\| > T$	$\|\|h_1(dB)\| - \|h_2(dB)\|\| \leq T$	Gain (dB)
1	$[\sqrt{0.1830} \quad \sqrt{0.8170}]$	$[\sqrt{0.4680} \quad \sqrt{0.5320}]$	9.38
2	$[\sqrt{0.1580} \quad \sqrt{0.8420}]$	$[\sqrt{0.4380} \quad \sqrt{0.5620}]$	9.91
3	$[\sqrt{0.1340} \quad \sqrt{0.8660}]$	$[\sqrt{0.4080} \quad \sqrt{0.5920}]$	10.32
4	$[\sqrt{0.1130} \quad \sqrt{0.8870}]$	$[\sqrt{0.3810} \quad \sqrt{0.6190}]$	10.60
5	$[\sqrt{0.0940} \quad \sqrt{0.9060}]$	$[\sqrt{0.3560} \quad \sqrt{0.6440}]$	10.73
6	$[\sqrt{\mathbf{0.0780}} \quad \sqrt{\mathbf{0.9220}}]$	$[\sqrt{\mathbf{0.3330}} \quad \sqrt{\mathbf{0.6670}}]$	**10.74**
7	$[\sqrt{0.0640} \quad \sqrt{0.9360}]$	$[\sqrt{0.3130} \quad \sqrt{0.6870}]$	10.65
8	$[\sqrt{0.0520} \quad \sqrt{0.9480}]$	$[\sqrt{0.2960} \quad \sqrt{0.7040}]$	10.50
9	$[\sqrt{0.0420} \quad \sqrt{0.9580}]$	$[\sqrt{0.2810} \quad \sqrt{0.7190}]$	10.31
10	$[\sqrt{0.0350} \quad \sqrt{0.9650}]$	$[\sqrt{0.2690} \quad \sqrt{0.7310}]$	10.12

Table 7.3: Soft-order g-mode 2 with 3 bits for phase and 2 bits for amplitude. The best gain is 14.34 dB, achieved for threshold equal to 6 dB.

$N_b = 5$ bits	Optimal Amplitude Weights		
Threshold T (dB)	$\|\|h_1(dB)\| - \|h_2(dB)\|\| > T$	$\|\|h_1(dB)\| - \|h_2(dB)\|\| \leq T$	Gain (dB)
1	$[\sqrt{0.2000} \quad \sqrt{0.8000}]$	$[\sqrt{0.4700} \quad \sqrt{0.5300}]$	11.56
2	$[\sqrt{0.1730} \quad \sqrt{0.8270}]$	$[\sqrt{0.4410} \quad \sqrt{0.5590}]$	12.48
3	$[\sqrt{0.1480} \quad \sqrt{0.8520}]$	$[\sqrt{0.4140} \quad \sqrt{0.5860}]$	13.28
4	$[\sqrt{0.1250} \quad \sqrt{0.8750}]$	$[\sqrt{0.3880} \quad \sqrt{0.6120}]$	13.91
5	$[\sqrt{0.1040} \quad \sqrt{0.8960}]$	$[\sqrt{0.3650} \quad \sqrt{0.6350}]$	14.27
6	$[\sqrt{\mathbf{0.0860}} \quad \sqrt{\mathbf{0.9140}}]$	$[\sqrt{\mathbf{0.3440}} \quad \sqrt{\mathbf{0.6560}}]$	**14.34**
7	$[\sqrt{0.0710} \quad \sqrt{0.9290}]$	$[\sqrt{0.3260} \quad \sqrt{0.6740}]$	14.18
8	$[\sqrt{0.0590} \quad \sqrt{0.9410}]$	$[\sqrt{0.3110} \quad \sqrt{0.6890}]$	13.89
9	$[\sqrt{0.0480} \quad \sqrt{0.9520}]$	$[\sqrt{0.2970} \quad \sqrt{0.7030}]$	13.52
10	$[\sqrt{0.0390} \quad \sqrt{0.9610}]$	$[\sqrt{0.2850} \quad \sqrt{0.7150}]$	13.14

Table 7.4: Soft-order g-mode 2 with 4 bits for phase and 2 bits for amplitude. The best gain is 16.22 dB, achieved for threshold equal to 6 dB.

$N_b = 6$ bits	Optimal Amplitude Weights		
Threshold T (dB)	$\|\|h_1(dB)\| - \|h_2(dB)\|\| > T$	$\|\|h_1(dB)\| - \|h_2(dB)\|\| \leq T$	Gain (dB)
1	$[\sqrt{0.2040} \quad \sqrt{0.7960}]$	$[\sqrt{0.4710} \quad \sqrt{0.5290}]$	12.42
2	$[\sqrt{0.1770} \quad \sqrt{0.8230}]$	$[\sqrt{0.4430} \quad \sqrt{0.5570}]$	13.54
3	$[\sqrt{0.1520} \quad \sqrt{0.8480}]$	$[\sqrt{0.4160} \quad \sqrt{0.5840}]$	14.58
4	$[\sqrt{0.1270} \quad \sqrt{0.8730}]$	$[\sqrt{0.3900} \quad \sqrt{0.6100}]$	15.52
5	$[\sqrt{0.1060} \quad \sqrt{0.8940}]$	$[\sqrt{0.3670} \quad \sqrt{0.6330}]$	16.08
6	$[\sqrt{\mathbf{0.0880}} \quad \sqrt{\mathbf{0.9120}}]$	$[\sqrt{\mathbf{0.3470}} \quad \sqrt{\mathbf{0.6530}}]$	**16.22**
7	$[\sqrt{0.0730} \quad \sqrt{0.9270}]$	$[\sqrt{0.3300} \quad \sqrt{0.6700}]$	16.02
8	$[\sqrt{0.0600} \quad \sqrt{0.9400}]$	$[\sqrt{0.3150} \quad \sqrt{0.6850}]$	15.59
9	$[\sqrt{0.0490} \quad \sqrt{0.9510}]$	$[\sqrt{0.3010} \quad \sqrt{0.6990}]$	15.04
10	$[\sqrt{0.0400} \quad \sqrt{0.9600}]$	$[\sqrt{0.2890} \quad \sqrt{0.7110}]$	14.52

Table 7.5: Comparison of soft-order g-mode 2 and traditional g-mode 2. As the number of available bits increases, soft-order g-mode 2 continues to provide gains in cases where the performance of traditional g-mode 2 begins to saturate.

	g-mode 2			soft-order g-mode 2		
Total Bits	Phase	Amplitude	Gain (dB)	Phase	Amplitude	Gain (dB)
3	2	1	8.73	1	2	6.10
4	3	1	10.70	2	2	10.74
5	4	1	11.34	3	2	14.34
6	5	1	11.59	4	2	16.22

Table 7.5 presents comparisons between the gains of altruistic g-mode 2 (1 bit for amplitude and N_p for phase) and the soft-order altruistic g-mode 2 presented above (2 bits for amplitude and $N_p - 1$ for phase) with threshold value equal to 6 dB. For g-mode 2, we apply the optimal amplitude weights $[\sqrt{0.2265} \ \sqrt{0.7735}]$ to the strongest and weakest antenna, respectively. We observe that g-mode 2 can provide similar or better performance than the soft-order g-mode 2 when the feedback message is up to 4 bits long (i.e., including phase and amplitude information) but after that point, increasing the phase resolution does not provide significant gains and performance becomes saturated. On the other hand, if the feedback message is at least 5 bits long, allocating two bits to the amplitude part of the feedback message provides gains of at least 3 dB against the respective g-mode 2.

7.2   Increasing the Number of Transmit Antennas

In the case of egoistic TBF, the algorithms of TSC, g-mode 1 and g-mode 2 are applicable to cases in which transmitters are equipped with more than two antennas. For g-mode 1, all phase modifications are made against a reference antenna, and, although this method is suboptimal and depends on the choice of reference antenna, gains can be achieved. For g-mode 2, amplitudes can be chosen in such a way that the strongest channel gains are favored. In the case of altruistic beamforming, though, adaptation of the algorithms is not as straightforward, except for TSC. Clearly g-mode 1 does not work, since directing all channel gains in phase opposition against just a single reference antenna is equivalent to a random outcome in the received signal. The best choice would be for the interfered MUE to test every possible beamforming vector of the predefined codebook to find the optimal one, according to equation (3.2). The problem with this brute force strategy is that it requires $|\mathcal{W}|$ beamforming vector tests, where $\mathcal{W}$ is the codebook containing all the possible beamforming vectors. For g-mode 1,

$$|\mathcal{W}| = 2^{N_p(N_t-1)}, \tag{7.1}$$

where N_p is the number of phase bits in the feedback message, and N_t is the number of transmit antennas. Therefore, when the number of antenna elements grows from N_t to $2N_t$, cardinality $|\mathcal{W}|$ increases rapidly by a factor of $2^{N_p N_t}$. Thus, finding the optimal weight requires heavy computations and possibly high delays, as transmitters become equipped with more and more antennas.

One option to bypass this problem is to group antenna elements in pairs. Then, application of altruistic g-mode 1 or g-mode 2 in their initial two-antenna form is possible, and the resulting channel gains from each pair are again grouped until only one channel gain remains. This algorithm requires multi-stage application of TBF, and can provide gains simply applying the original two-antenna algorithms multiple times. With this scheme, the gains are suboptimal, but the advantage is its more practical implementation against the brute force method mentioned above.

We will consider the case where transmitters are equipped with $N_t = 4$ transmit antennas. Antennas are not ranked according to their channel gain amplitude orders, but are randomly grouped into two pairs. Then, in the first stage, the same altruistic TBF method is applied to each pair separately. The outcome is

Table 7.6: Interference Mitigation for the case of four transmit antennas by grouping antennas in pairs and applying altruistic TBF in two stages.

Antennas 1 - 2	Bits	Antennas 3 - 4	Bits	Combination	Bits	SNR(dB)	Total Bits
TSC	1	TSC	1	TSC	1	6.04	3
TSC	1	TSC	1	g-mode 1	2	8.32	4
TSC	1	TSC	1	g-mode 1	3	9.35	5
TSC	1	TSC	1	g-mode 2	3	11.71	5
TSC	1	TSC	1	g-mode 2	4	13.67	6
g-mode 1	2	g-mode 1	2	TSC	1	8.67	5
g-mode 1	2	g-mode 1	2	g-mode 1	2	10.3	6
g-mode 1	3	g-mode 1	3	TSC	1	10.3	7
g-mode 1	2	g-mode 1	2	g-mode 1	3	11.13	7
g-mode 1	2	g-mode 1	2	g-mode 2	3	13.98	7
g-mode 2	3	g-mode 2	3	TSC	1	11.87	7
g-mode 1	3	g-mode 1	3	g-mode 1	2	10.58	8
g-mode 1	2	g-mode 1	2	g-mode 2	4	15.81	8
g-mode 2	3	g-mode 2	3	g-mode 1	2	13.91	8
g-mode 1	3	g-mode 1	3	g-mode 1	3	11.14	9
g-mode 1	3	g-mode 1	3	g-mode 2	3	14.63	9
g-mode 2	4	g-mode 2	4	TSC	1	14.20	9
g-mode 2	3	g-mode 2	3	g-mode 1	3	14.86	9
g-mode 2	3	g-mode 2	3	g-mode 2	3	17.39	9
g-mode 1	3	g-mode 1	3	g-mode 2	4	16.01	10
g-mode 2	4	g-mode 2	4	g-mode 1	2	15.29	10
g-mode 2	3	g-mode 2	3	g-mode 2	4	19.31	10
g-mode 2	4	g-mode 2	4	g-mode 1	3	16.05	11
g-mode 2	4	g-mode 2	4	g-mode 2	3	19.14	11
g-mode 2	4	g-mode 2	4	g-mode 2	4	20.81	12

one modified channel gain from each pair. The two new channel gains are again grouped into one pair and an altruistic TBF method is applied. The resulting beamforming gains from different combinations and resolutions of TBF methods can be seen in Table 7.6.

The option of using TSC in two stages is not efficient, since direct TSC for

4 antennas provides the same 6 dB gain with only 2 bits. The most efficient combinations require the presence of g-mode 2, at least in the last stage. Comparisons with two-antenna schemes prove the efficiency of having more antennas. With as low as 5 feedback bits, performance of traditional two-antenna g-mode 2 with 4 bits (approximately 10.7 dB) is already surpassed (11.71 dB) and gains continue to rise as the number of available feedback bits increases. The highest gain is approximately 20.81 dB and requires exclusive usage of g-mode 2 with 4 bits for each pair. In total, 12 bits are required for the feedback message. It is worth noting that a similar gain could be achieved with 9 bits (21.45 dB), if brute force search was used to repeatedly test all $8^3 = 512$ beamforming vectors of the g-mode 1 codebook for four antennas. Therefore, the proposed scheme has the advantage of not demanding time-consuming computations at the receiver side, but the trade-off is that the feedback channel rate should be quite higher.

Chapter 8

Conclusions and Future Work

Cross-layer interference scenarios in two-tier heterogeneous networks could negatively influence the overall network performance. The bottleneck is usually the downlink direction, since macro base stations are typically considered as primary infrastructure. In this thesis, we have presented results about the performance improvements that altruistic TBF can introduce to an MUE which is heavily interfered by a group of FBSs.

8.1 Conclusions

We have derived analytical formulas for the upper bound of the received SINR at the MUE, in cases where a single dominant interferer applies altruistic TBF with perfect phase resolution. Results dictate that performance close to the upper bound can practically be achieved by using as low as 4 feedback bits, instead of infinite.

We have investigated the case of multiple interferers, and derived the respective analytical results for the SINR improvements at the MUE. We deduce that it is not vital to cancel every interferer, but only the cluster of closest interferers. In practice, this number will typically be quite low, since FBSs are not installed in every apartment and do not transmit 100 % of the time. Thus, altruistic beamforming can provide great improvements with minimal sacrifices.

Finally, we have investigated and presented simulation results about possible extensions of the altruistic beamforming methods. By adding one more amplitude bit in g-mode 2, we have observed that performance can be improved significantly, but only when the feedback message is at least 5 bits long. Similarly, we have

tested an interference mitigation scheme that groups antennas in pairs and performs altruistic TBF methods for each pair. This method is suboptimal, but can provide similar gains to the two-antenna case with straightforward implementation.

8.2   Future Work

The work presented in this thesis could be extended in future studies, in the following possible research directions:

1. Instead of including just one beamforming vector, the feedback message from the interfered MUE towards each interferer FBS could include multiple beamforming vectors that are sufficient for combating received interference at the MUE (e.g. as in [67]). Then, the interferer FBS is not forced to behave altruistic, but has the capability to choose the beamforming vector that degrades performance for its own FUE as little as possible. The number of beamforming vectors that are fed back determines the level of bargaining between the performance improvement of the MUE and the performance degradation of the respective FUE. Further analysis and application of such a feedback scheme to various two-tier scenarios is of great interest.

2. For the two-antenna case of soft-order g-mode 2 with 2 bits of amplitude feedback, analytical work could be carried out for the derivation of the exact amplitude weights that minimize interference, given the optimal threshold value for the amplitude difference. Furthermore, the performance of g-mode 2 with more than 2 bits reserved for amplitude could be investigated.

3. When transmitters are equipped with more than two transmit antennas, useful approximations could be derived for efficient modeling of the probability distribution of the received SNR, when the goal is combating interference by grouping the antenna elements. In addition, investigation of new methods for direct interference mitigation without grouping of antenna elements could be considered.

4. When transmitters are equipped with more than two transmit antennas, useful approximations could be derived for efficient modeling of the probability distribution of the received SNR, when the goal is combating in-

terference by grouping the antenna elements. In addition, investigation of new methods for direct interference mitigation without grouping of antenna elements could be considered.

Bibliography

[1] Ericsson, *On the Pulse of the Networking Society*, White paper, Jun. 2012.

[2] Qualcomm Incorporated, *LTE Advanced: Heterogeneous Networks*, White paper, Jan. 2011.

[3] H. Liang, J. I. Payne, H. S. Kim, *Femto-Cells: Problem or Solution? A Network Cost Analysis*, in Proc. IEEE Global Telecommunications Conference, pp. 1-6, Dec. 2011.

[4] D. Lopez-Perez, I. Guvenc, G. de la Roche, M. Kountouris, T. Q. S. Quek, J. Zhang, *Enhanced Intercell Interference Coordination Challenges in Heterogeneous Networks*, IEEE Wireless Communications, vol. 41, no. 2, pp. 22-30, Jun. 2011.

[5] A. Bou Saleh, S. Redana, B. Raaf, J. Hämäläinen, *Comparison of Relay and Pico eNB Deployments in LTE-Advanced*, in Proc. IEEE Vehicular Technology Conference, pp. 1-5, Sep. 2009.

[6] S. Kaimaletu, R. Krishnan, S. Kalyani, N. Akhtar, B. Ramamurthi, *Cognitive Interference Management in Heterogeneous Femto-Macro Cell Networks*, in Proc. IEEE International Conference on Communications, pp. 1-6, Jun. 2011.

[7] Femto Forum, *Femto Forum Summary Report: Interference Management in UMTS Femtocells*, White paper, Feb. 2010.

[8] D. J. Love, R. W. Heath, V. K. N. Lau, D. Gesbert, B. D. Rao, M. Andrews, *An Overview of Limited Feedback in Wireless Communication Systems*, IEEE Journal on Selected Areas in Communications, vol. 26, no. 8, pp. 1341-1365, Oct. 2008.

[9] V. Chandrasekhar, J. G. Andrews, T. Muharemovic, Z. Shen, A. Gatherer, *Power control in two-tier femtocell networks*, IEEE Trans. on Wireless Comm., vol. 8, no. 8, pp. 4316-4328, Aug. 2009.

[10] C. Karaiskos, A. A. Dowhuszko, J. Hämäläinen, *Performance of Altruistic Beamforming for Mitigation of Multiple Cross-layer Interference Sources*, submitted to IEEE International Conference on Communications 2013.

[11] P. W. C. Chan, E. S. Lo, R. R. Wang, E. K. S. Au, V. K. N. Lau, R. S. Cheng, W. Ho Mow, R.D. Murch, and K. Ben Letaief, *The Evolution of 4G Networks: FDD or TDD?*, IEEE Communications Magazine, vol. 44, no. 12, pp. 42-50, Dec. 2006.

[12] J. H. Winters, *The Diversity Gain of Transmit Diversity in Wireless Systems with Rayleigh Fading*, IEEE Transactions on Vehicular Technology, pp. 1121-1125, Feb. 1998.

[13] Motorola, *Orthogonal Transmit Diversity for Direct Spread CDMA*, ETSI Contribution, Sep. 1997.

[14] B. Hochwald, T. L. Marzetta, C.B. Papadias, *The Diversity Gain of Transmit Diversity in Wireless Systems with Rayleigh Fading*, IEEE Journal on Selected Areas in Communications, vol. 19, no. 1, pp. 48-60, Feb. 2001.

[15] A. Heroike, F. Adachi, N. Nakajima, *Combined Effects of Phase Sweeping Transmitter Diversity and Channel Coding*, IEEE Transactions on Vehicular Technology, vol. 41, no. 2, pp. 170-176, May 1992.

[16] Samsung, *Proposal for Downlink Time Switched Transmission Diversity*, ETSI Contribution, Germany 1998.

[17] Z. Liu, G. B. Giannakis, S. Zhou, B. Muquet, *Space Time Coding for Broadband Wireless Communications*, Wireless Communications and Mobile Computing, vol. 1, no. 1, pp. 35-53, Jan. 2001.

[18] S. M. Alamouti, *A Simple Transmit Diversity Technique for Wireless Communications*, IEEE Journal on Selected Areas in Communications, vol. 16, no. 8, pp. 1451-1458, Oct. 1998.

[19] A. G. Dabak, S. Hosur, T. Schmidl, C. Sengupta, *A Comparison of the Open Loop Transmit Diversity Schemes for Third Generation Wireless Systems*,

in Proc. Wireless Communications and Networking Conference, pp. 437-442, Sep. 2000.

[20] R. T. Derryberry, S. D. Gray, D. M. Ionescu, G. Mandyam, B. Raghothaman, *Transmit Diversity in 3G CDMA Systems*, IEEE Communications Magazine, vol. 40, no. 4, pp. 68-75, Apr. 2002.

[21] *MIMO Techniques in WiMAX and LTE: a Feature Overview*, IEEE Communications Magazine, vol. 48, no. 5, pp. 86-92, May 2010.

[22] E. Visotsky, U. Madhow, *SpaceTime Transmit Precoding with Imperfect Feedback*, IEEE Transactions on Information Theory, vol. 47, no. 6, Sep. 2001.

[23] S. A. Jafar, S. Vishwanath, A. J. Goldsmith, *Channel Capacity and Beamforming for Multiple Transmit and Receive Antennas with Covariance Feedback*, in Proc. IEEE International Conference on Communications, vol. 7, pp. 2266-2270, Jun. 2001.

[24] E. A. Jorswieck and H. Boche, *Channel Capacity and Capacity-Range of Beamforming in MIMO Wireless Systems under Correlated Fading with Covariance Feedback*, IEEE Transactions on Wireless Communications, vol. 3, pp. 1543-1553, Sep. 2004.

[25] S. Srinivasa and S. A. Jafar, *Capacity of the Isotropic Fading Multiple Antenna Downlink with Magnitude Feedback*, in Proc. IEEE Vehicular Technology Conference, vol. 3, pp. 2001-2005, Sep. 2004.

[26] K. K. Mukkavilli, A. Sabharwal, E. Erkip and B. Aazhang, *On Beamforming with Finite Rate Feedback in Multiple Antenna Systems*, IEEE Transactions on Information Theory, vol. 49, pp. 2562-2579, Oct. 2003.

[27] P. Xia, S. Zhou and G. B. Giannakis, *Design and Analysis of Transmit Beamforming Based on Limited-Rate Feedback*, IEEE Transactions on Signal Processing, vol. 54, pp. 1853-1863, May 2005.

[28] S. Srinivasa and S. A. Jafar, *Vector Channel Capacity with Quantized Feedback*, in Proc. IEEE International Conference on Communications, vol. 4, pp. 2674-2678, May 2005.

[29] J. C. Roh and B. D. Rao, *Multiple Antenna Channels with Partial Channel State Information at the Transmitter*, IEEE Transactions on Wireless Communications, vol. 3, pp. 677-688, Mar. 2004.

[30] J. Hämäläinen, *Performance Analysis of Multi-antenna and Multi-user Methods for 3G and Beyond*, PhD Dissertation, Espoo, 2007.

[31] S. Srinivasa, *The Optimality of Beamforming: A Unified View*, in Proc. Global Telecommunications Conference, Dec. 2005.

[32] N. R. Sollenberger, *Diversity and Automatic Link Transfer for a TDMA Wireless Access Link*, in Proc. IEEE Global Telecommunications Conference, vol. 1, pp. 532-536, Dec. 1993.

[33] A. Narula, M. J. Lopez, M. D. Trott, and G. W. Wornell, *Efficient Use of Side Information in Multiple-antenna Data Transmission over Fading Channels*, IEEE Journal on Selected Areas in Communications, vol. 16, pp. 1423-1436, Oct. 1998.

[34] D. J. Love, R. W. Heath Jr., T. Strohmer, *Grassmannian Beamforming for Multiple-Input Multiple-Output Wireless Systems*, in Proc. IEEE International Conference on Communications, vol. 4, pp. 2618-2622, May 2003.

[35] J. C. Roh, B. D. Rao, *Transmit Beamforming in Multiple-Antenna Systems With Finite Rate Feedback: A VQ-Based Approach*, IEEE Transactions on Information Theory, vol. 52, no. 3, pp. 1101-1112, Mar. 2006.

[36] A. Hottinen, O. Tirkkonen, R. Wichman, *Multi-antenna Transceiver Techniques for 3G and Beyond*, Wiley, 2003.

[37] J. Hämäläinen, R. Wichman, A. A. Dowhuszko, G. Corral-Briones, *Capacity of Generalized UTRA FDD Closed-Loop Transmit Diversity Modes*, Wireless Personal Communications: An International Journal archive vol. 54, no. 3, pp. 467-484, Aug. 2010.

[38] A. Hottinen and R. Wichman, *Transmit Diversity by Antenna Selection in CDMA Downlink*, in Proc. IEEE International Symposium on Spread Spectrum Techniques and Applications, vol. 3, pp. 767-770, Sep. 1998.

[39] J. Hämäläinen, R. Wichman, *Performance Analysis of Closed-loop Transmit Diversity in the Presence of Feedback Errors*, in Proc. IEEE International

Symposium on Personal, Indoor and Mobile Radio Communications, vol. 5, pp. 2297-2301, Sep. 2002.

[40] R. W. Heath Jr. and A. Paulraj, *A Simple Scheme for Transmit Diversity Using Partial Channel Feedback*, in Proc. Asilomar Conference on Signals, Systems, Computers, pp. 1073-1078, Nov. 1998.

[41] D. J. Love, R. W. Heath Jr., *Equal Gain Transmission in Multiple-Input Multiple-Output Wireless Systems*, IEEE Transactions on Communications, vol. 51, no. 7, pp. 1102-1110, Jul. 2003.

[42] J. Hämäläinen, R. Wichman, *Closed-Loop Transmit Diversity for FDD WCDMA Systems*, in Proc. Asilomar Conference on Signals, Systems and Computers, vol. 1, pp. 111-115, Oct. 2000.

[43] H. S. Dhillon, R. K. Ganti, F. Baccelli, J. G. Andrews, *Modeling and Analysis of K-Tier Downlink Heterogeneous Cellular Networks*, IEEE Journal on Selected Areas in Communications, vol. 30, no. 3, pp. 550-560, Apr. 2012.

[44] D. Lopez-Perez, A. Valcarce, G. De La Roche, E. Liu, J. Zhang, *Access Methods to WiMAX Femtocells: A Downlink System-level Case Study*, in Proc. IEEE International Conference on Communication Systems, pp. 1657-1662, Nov. 2008.

[45] G. de la Roche, A. Valcarce, D. Lopez-Perez, J. Zhang, *Access Control Mechanisms for Femtocells*, IEEE Communications Magazine, vol. 48, no. 1, pp. 33-39, Jan. 2010.

[46] 3rd Generation Partnership Project, Technical Specification Group Radio Access Network, *3G Home NodeB Study Item Technical Report*, 3GPP TR 25.820 V8.0.0 (2008-03).

[47] 3rd Generation Partnership Project, Technical Specification Group Radio Access Network, *FDD Home eNode B (HeNB) Radio Frequency (RF) Requirements Analysis*, 3GPP TR 36.921 V9.0.0 (2010-03).

[48] M. Yavuz, F. Meshkati, S. Nanda, A. Pokhariyal, N. Johnson, B. Raghothaman, A. Richardson, *Interference Management and Performance Analysis of UMTS/HSPA+ Femtocells*, IEEE Communications Magazine, vol. 47, no. 9, pp. 102-109, Sep. 2009.

[49] Qualcomm Incorporated, *R1-102350: Assessment of Rel-8/9 Techniques Available to Cope with Harsh Interference Conditions*, 3GPP TSG-RAN WG1 60, Apr. 2010.

[50] CEWiT, *R1-104106: Cognitive Interference Management for Femto-Macro Scenarios*, 3GPP TSG RAN1 61bis meeting, Jul. 2010.

[51] V. Chandrasekhar, J. G. Andrews, *Spectrum Allocation in Two-tier Networks*, in Proc. Asilomar Conference on Signals, Systems, Computers, pp. 1583-1587, Oct. 2008.

[52] Nokia Siemens Networks, Nokia, *R1-101924: Macro+HeNB Performance with Escape Carrier or Dynamic Carrier Selection*, 3GPP TSG RAN WG1 60bis Meeting, Apr. 12-16, 2010.

[53] CATT, ITRI, *R1-101786: Interference Mitigation via Direction Information in Het-Net*, 3GPP TSG RAN WG1 meeting 60bis, Apr. 2010.

[54] S. Rangan, *Femto-Macro Cellular Interference Control with Subband Scheduling and Interference Cancellation*, in Proc. IEEE Globecom Workshop on Femtocell Networks, pp. 1-9, Jul. 2010.

[55] Motorola, *R1-101121: HeNB Interference Management*, 3GPP TSG-RAN WG1 Meeting 60, Feb. 2010.

[56] G. Boudreau, J. Panicker, N. Guo, R. Chang, N. Wang, S. Vrzic, *Interference Coordination and Cancellation for 4G Networks*, IEEE Communications Magazine, vol. 47, no. 4, pp. 74-81, Apr. 2009.

[57] S. Kaimaletu, R. Krishnan, S. Kalyani, N. Akhtar, B. Ramamurthi, *Cognitive Interference Management in Heterogeneous Femto-Macro Cell Networks*, in Proc. IEEE International Conference on Communications, pp. 1-6, Jun. 2011.

[58] NTT DOCOMO Incorporated, *R1-083686: Views on Coordinated Multipoint Transmission/Reception in LTE-Advanced*, 3GPP TSG RAN WG1 Meeting 54bis, Sep. 2008.

[59] Ericsson, *R1-082469: LTE-Advanced-Coordinated Multipoint Transmission/Reception*, TSG-RAN WG1 53bis, Jul. 2008.

[60] Huawei, *R1-083049: Consideration on CoMP for LTE-Advanced*, 3GPP TSG RAN WG1 54, Aug. 2008.

[61] A. Papadogiannis, E. Hardouin, D. Gesbert, *A Framework for Decentralising Multi-Cell Cooperative Processing on the Downlink*, in Proc. IEEE Global Communications Conference Workshops, pp. 1-5, Dec. 2008.

[62] N. Seifi, M. Viberg, R. W. Heath, J. Zhang, and M. Coldrey, *Coordinated Single-cell vs Multi-cell Transmission with Limited-capacity Backhaul*, in Proc. Asilomar Conference on Signals, Systems, Computers, pp. 1217-1221, Nov. 2010.

[63] CELTIC/CP5-026 WINNER+, *D1.4 Initial Report on Advanced Multiple Antenna Systems*, Technical Report, Jan. 2009.

[64] I. F. Akyildiz, D. M. Gutierrez-Estevez, E. C. Reyes, *The Evolution to 4G Cellular Systems: LTE-Advanced*, Physical Communication, vol. 3, no. 4, pp. 217-244, Dec. 2010.

[65] D. Lee, H. Seo, B. Clerckx, E. Hardouin, D. Mazzarese, S. Nagata, K. Sayana, *Coordinated Multipoint Transmission and Reception in LTE-Advanced: Deployment Scenarios and Operational Challenges*, IEEE Communications Magazine, vol. 50, no. 2, pp. 148-155, Feb. 2012.

[66] M. Husso, J. Hämäläinen, R. Jäntti, J. Li, E. Mutafungwa, R. Wichman, Z. Zheng and A. M. Wyglinski, *Performance of Practical Transmit Beamforming Methods for Interference Suppression in Closed-access Femtocells*, EURASIP Journal on Wireless Communications and Networking, pp. 1-12, Jun. 2010.

[67] A. Elsherif, A. M. Ahmedin, Z. Ding, X. Liu, *Adaptive precoding for femtocell interference mitigation*, in Proc. IEEE International Conference on Communications, Jul. 2012.

[68] V. Chandrasekhar, J. G. Andrews, T. Muharemovic, Z. Shen, A. Gatherer, *Power Control in Two-Tier Femtocell Networks*, IEEE Transactions on Wireless Communications, vol. 8, no. 8, pp. 4316-4328, Aug. 2009.

[69] Alcatel-Lucent, picoChip Designs, Vodafone, *R4-092042: Simulation Assumptions and Parameters for FDD HeNB RF Requirements*, 3GPP TSG RAN WG4 (Radio) Meeting 51, May 2009.

[70] V. Krishnan, *Probability and Random Processes*, Wiley Press, Chapter 13, Section 4, pp. 233-238, 2006.

[71] I. S. Gradshtein, I. M. Ryzhik, A. Jeffrey, D. Zwillinger, *Table of Integrals, Series, And Products 7th edition*, Elsevier Academic Press, 2007.

[72] A. A. Dowhuszko, G. Corral-Briones, J. Hämäläinen, and R. Wichman, *On Throughput-Fairness Tradeoff in Virtual MIMO Systems with Limited Feedback*, EURASIP Journal on Wireless Communications and Networking, pp. 1-17, Jan. 2009.

[73] A. A. Dowhuszko, M. Husso, J. Li, J. Hämäläinen, Z. Zheng, *Performance of Practical Transmit Beamforming Methods for Interference Suppression in Closed-access Femtocells*, Future Network and Mobile Summit (FutureNetw), pp. 1-12, Jun. 2011.

[74] S. Ross, *Introduction to Probability Models*, 9th ed., Elsevier Academic Press, Chapter 5, Section 2.4, pp. 298-300, 2007.

[75] A. Papoulis, *Probability, random variables, and stochastic processes*, 3rd ed., McGraw-Hill Int. Ed., 1991.

Appendix A

Perfect Phase Feedback: PDF of Egoistic Case

In this section, we present the procedure to obtain the PDF of

$$X = \bar{\gamma}_{\mathrm{x}} |\mathbf{h_x} \cdot \hat{\mathbf{w}}_x|^2_{max} = \frac{\bar{\gamma}_{\mathrm{x}}}{2}(|\mathrm{h_{x1}}| + |\mathrm{h_{x2}}|)^2, \qquad (A.1)$$

following the procedure found in [70] for determining the PDF of an RV which is a function of multiple RVs.

We have assumed that $\mathrm{h_{x1}}$, $\mathrm{h_{x2}}$ are complex Gaussian RVs with zero mean and unitary variance, so $\mathrm{Re}\{\mathrm{h_{x1}}\}, \mathrm{Re}\{\mathrm{h_{x2}}\} \sim \mathcal{N}(0, \frac{1}{2})$ and $\mathrm{Im}\{\mathrm{h_{x1}}\}, \mathrm{Im}\{\mathrm{h_{x2}}\} \sim \mathcal{N}(0, \frac{1}{2})$. Thus, each amplitude $|\mathrm{h_{x1}}|$ and $|\mathrm{h_{x2}}|$ follows a Rayleigh distribution with $\sigma = \frac{1}{\sqrt{2}}$. For simplicity, notation of the above RVs will be $\mathrm{U} = |h_{x1}|$ and $\mathrm{V} = |h_{x2}|$. Then, we need to prove the PDF of $\mathrm{X} = \frac{\bar{\gamma}_{\mathrm{x}}}{2}(U + V)^2$.

The PDFs of U and V are given by

$$f_U(u) = \frac{u}{\sigma^2} e^{(-\frac{u^2}{2\sigma^2})}, \qquad u > 0, \qquad (A.2)$$

$$f_V(\nu) = \frac{\nu}{\sigma^2} e^{(-\frac{\nu^2}{2\sigma^2})}, \qquad \nu > 0, \qquad (A.3)$$

respectively. Since U and V are independent, their joint PDF is given by

$$f_{U,V}(u,\nu) = \frac{u\nu}{\sigma^4} e^{(-\frac{u^2+\nu^2}{2\sigma^2})}, \qquad u, \nu > 0. \qquad (A.4)$$

In order to simplify the derivation of $f_X(x)$, we will use the auxiliary random variable $\mathrm{W} = \mathrm{U}$, so that we have two functions of two random variables. Solving $\mathrm{x} = \frac{\bar{\gamma}_{\mathrm{x}}}{2}(u + \nu)^2$ for ν, setting $u = w$ and taking into account that all RVs are

positive, we obtain the only acceptable solution $\nu_1 = \sqrt{\frac{2x}{\bar{\gamma}_x}} - w$, with $0 < w < \sqrt{\frac{2x}{\bar{\gamma}_x}}$. The Jacobian matrix and its absolute determinant are

$$J = \begin{bmatrix} \bar{\gamma}_x(u+\nu) & \bar{\gamma}_x(u+\nu) \\ 1 & 0 \end{bmatrix} \qquad ||J|| = |u+\nu| = \sqrt{2\bar{\gamma}_x x}. \qquad (A.5)$$

The joint density function $f_{XW}(x,w)$ is given by

$$
\begin{aligned}
f_{XW}(x,w) &= \frac{f_{UV}\left(w, \sqrt{\frac{2x}{\bar{\gamma}_x}} - w\right)}{||J||} \\
&= \frac{w\left(\sqrt{\frac{2x}{\bar{\gamma}_x}} - w\right)}{\sigma^4 \sqrt{2\bar{\gamma}_x x}} e^{\frac{-\left(w^2 + \left(\sqrt{\frac{2x}{\bar{\gamma}_x}} - w\right)^2\right)}{2\sigma^2}} \\
&= \frac{w\sqrt{\frac{2x}{\bar{\gamma}_x}} - w^2}{\sigma^4 \sqrt{2\bar{\gamma}_x x}} e^{\frac{-\left(w^2 + w^2 + \frac{2x}{\bar{\gamma}_x} - 2w\sqrt{\frac{2x}{\bar{\gamma}_x}}\right)}{2\sigma^2}} \\
&= \frac{-\left(w^2 - w\sqrt{\frac{2x}{\bar{\gamma}_x}} + \frac{2x}{4\bar{\gamma}_x}\right) + \frac{2x}{4\bar{\gamma}_x}}{\sigma^4 \sqrt{2\bar{\gamma}_x x}} e^{\frac{-\left(w^2 - w\sqrt{\frac{2x}{\bar{\gamma}_x}} + \frac{2x}{2\bar{\gamma}_x}\right)}{\sigma^2}} \\
&= \frac{-\left(w - \frac{\sqrt{2x}}{2\sqrt{\bar{\gamma}_x}}\right)^2 + \frac{2x}{4\bar{\gamma}_x}}{\sigma^4 \sqrt{2\bar{\gamma}_x x}} e^{\frac{-\left(w - \frac{\sqrt{2x}}{2\sqrt{\bar{\gamma}_x}}\right)^2 - \frac{2x}{4\bar{\gamma}_x}}{\sigma^2}} \\
&= \frac{e^{-\frac{x}{2\bar{\gamma}_x \sigma^2}}}{\sqrt{2\bar{\gamma}_x x}} \left(\frac{-\left(w - \frac{\sqrt{2x}}{2\sqrt{\bar{\gamma}_x}}\right)^2}{\sigma^4} e^{\frac{-\left(w - \frac{\sqrt{2x}}{2\sqrt{\bar{\gamma}_x}}\right)^2}{\sigma^2}} + \frac{x}{2\bar{\gamma}_x \sigma^4} e^{\frac{-\left(w - \frac{\sqrt{2x}}{2\sqrt{\bar{\gamma}_x}}\right)^2}{\sigma^2}}\right). \quad (A.6)
\end{aligned}
$$

In order to derive $f_X(x)$, we now integrate over all w, with $0 < w < \sqrt{\frac{2x}{\bar{\gamma}_x}}$, i.e.,

$$
f_X(x) = \frac{e^{-\frac{x}{2\bar{\gamma}_x \sigma^2}}}{\sqrt{2\bar{\gamma}_x x}} \left(\int_0^{\sqrt{\frac{2x}{\bar{\gamma}_x}}} \frac{-\left(w - \frac{\sqrt{2x}}{2\sqrt{\bar{\gamma}_x}}\right)^2}{\sigma^4} e^{\frac{-\left(w - \frac{\sqrt{2x}}{2\sqrt{\bar{\gamma}_x}}\right)^2}{\sigma^2}} dw + \frac{x}{2\bar{\gamma}_x \sigma^4} e^{\frac{-\left(w - \frac{\sqrt{2x}}{2\sqrt{\bar{\gamma}_x}}\right)^2}{\sigma^2}} dw\right)
$$

$$(A.7)$$

$$= \frac{e^{-\frac{x}{2\bar{\gamma}_x \sigma^2}}}{\sqrt{2\bar{\gamma}_x x}} (A + B). \qquad (A.8)$$

We will compute the integrals separately, using variable substitution:

$$A = \int_0^{\sqrt{\frac{2x}{\bar{\gamma}_x}}} \frac{-(w - \frac{\sqrt{2x}}{2\sqrt{\bar{\gamma}_x}})^2}{\sigma^4} e^{\frac{-(w - \frac{\sqrt{2x}}{2\sqrt{\bar{\gamma}_x}})^2}{\sigma^2}} dw$$

$$\left(\text{variable substitution: } k = \frac{(w - \frac{\sqrt{2x}}{2\sqrt{\bar{\gamma}_x}})}{\sigma} \right)$$

$$= \int_{-\frac{\sqrt{2x}}{2\sqrt{\bar{\gamma}_x}\sigma}}^{\frac{\sqrt{2x}}{2\sqrt{\bar{\gamma}_x}\sigma}} \frac{-k^2}{\sigma^2} e^{-k^2} \sigma dk$$

$$= -\frac{1}{\sigma} \int_{-\frac{\sqrt{2x}}{2\sqrt{\bar{\gamma}_x}\sigma}}^{\frac{\sqrt{2x}}{2\sqrt{\bar{\gamma}_x}\sigma}} k^2 e^{-k^2} dk$$

$$= -\frac{1}{\sigma} \left(\frac{1}{4}\sqrt{\pi} \, \text{erf}(k) - \frac{1}{2} e^{-k^2} k \right) \Bigg|_{-\frac{\sqrt{2x}}{2\sqrt{\bar{\gamma}_x}\sigma}}^{\frac{\sqrt{2x}}{2\sqrt{\bar{\gamma}_x}\sigma}}$$

$$= -\frac{1}{\sigma} \left[\frac{1}{2}\sqrt{\pi} \, \text{erf}\left(\frac{\sqrt{2x}}{2\sqrt{\bar{\gamma}_x}\sigma} \right) - \frac{\sqrt{2x}}{2\sqrt{\bar{\gamma}_x}\sigma} e^{-\frac{x}{2\bar{\gamma}_x\sigma^2}} \right]. \tag{A.9}$$

$$B = \int_0^{\sqrt{\frac{2x}{\bar{\gamma}_x}}} \frac{x}{2\bar{\gamma}_x\sigma^4} e^{\frac{-(w - \frac{\sqrt{2x}}{2\sqrt{\bar{\gamma}_x}})^2}{\sigma^2}} dw$$

$$\left(\text{variable substitution: } k = \frac{(w - \frac{\sqrt{2x}}{2\sqrt{\bar{\gamma}_x}})}{\sigma} \right)$$

$$= \frac{x}{2\bar{\gamma}_x\sigma^4} \int_{-\frac{\sqrt{2x}}{2\sqrt{\bar{\gamma}_x}\sigma}}^{\frac{\sqrt{2x}}{2\sqrt{\bar{\gamma}_x}\sigma}} e^{-k^2} \sigma dk$$

$$= \frac{x\sqrt{\pi}}{4\bar{\gamma}_x\sigma^3} \frac{2}{\sqrt{\pi}} \int_{-\frac{\sqrt{2x}}{2\sqrt{\bar{\gamma}_x}\sigma}}^{\frac{\sqrt{2x}}{2\sqrt{\bar{\gamma}_x}\sigma}} e^{-k^2} dk$$

$$= \frac{x\sqrt{\pi}}{4\bar{\gamma}_x\sigma^3} \left[\text{erfc}\left(-\frac{\sqrt{2x}}{2\sqrt{\bar{\gamma}_x}\sigma} \right) - \text{erfc}\left(\frac{\sqrt{2x}}{2\sqrt{\bar{\gamma}_x}\sigma} \right) \right]$$

$$= \frac{x\sqrt{\pi}}{2\bar{\gamma}_x\sigma^3} \text{erf}\left(\frac{\sqrt{2x}}{2\sqrt{\bar{\gamma}_x}\sigma} \right). \tag{A.10}$$

Therefore,

$$f_X(x) = \frac{e^{-\frac{x}{2\bar{\gamma}_x\sigma^2}}}{2\sigma\sqrt{2\bar{\gamma}_x x}} \left[-\sqrt{\pi} \, \text{erf}\left(\frac{\sqrt{2x}}{2\sqrt{\bar{\gamma}_x}\sigma} \right) + \frac{\sqrt{2x}}{\sqrt{\bar{\gamma}_x}\sigma} e^{-\frac{x}{2\bar{\gamma}_x\sigma^2}} + \frac{x\sqrt{\pi}}{\bar{\gamma}_x\sigma^2} \text{erf}\left(\frac{\sqrt{2x}}{2\sqrt{\bar{\gamma}_x}\sigma} \right) \right]. \tag{A.11}$$

Now, derivation of the PDF of (A.1) is possible, by substitution of $\sigma = \frac{1}{\sqrt{2}}$:

$$f_X(x) = \frac{e^{-\frac{x}{\bar{\gamma}_x}}}{2\sqrt{x\bar{\gamma}_x}} \left[-\sqrt{\pi}\ \mathrm{erf}\left(\sqrt{\frac{x}{\bar{\gamma}_x}}\right) + 2\sqrt{\frac{x}{\bar{\gamma}_x}}e^{-\frac{x}{\bar{\gamma}_x}} + \frac{2x\sqrt{\pi}}{\bar{\gamma}_x}\mathrm{erf}\left(\sqrt{\frac{x}{\bar{\gamma}_x}}\right) \right]. \quad \text{(A.12)}$$

Appendix B

Perfect Phase Feedback: Calculation of SINR

In order to find $F_Z(z) = \int_1^\infty F_X(zt) f_Y(t-1) dt$, the following integrals must be solved and added:

①　$\displaystyle\int_1^\infty -\sqrt{\pi}\frac{\sqrt{zt}}{\sqrt{\bar{\gamma}_x}}e^{-\frac{zt}{\bar{\gamma}_x}}\mathrm{erf}\left(\frac{\sqrt{zt}}{\sqrt{\bar{\gamma}_x}}\right)\frac{e^{-\frac{t-1}{\bar{\gamma}_y}}}{2\sqrt{\bar{\gamma}_y(t-1)}}\sqrt{\pi}dt,$　　(B.1)

②　$\displaystyle\int_1^\infty \sqrt{\pi}\frac{\sqrt{zt}}{\sqrt{\bar{\gamma}_x}}e^{-\frac{zt}{\bar{\gamma}_x}}\mathrm{erf}\left(\frac{\sqrt{zt}}{\sqrt{\bar{\gamma}_x}}\right)\frac{e^{-\frac{t-1}{\bar{\gamma}_y}}}{2\sqrt{\bar{\gamma}_y(t-1)}}\sqrt{\pi}\,\mathrm{erf}\left(\frac{\sqrt{t-1}}{\sqrt{\bar{\gamma}_y}}\right)dt,$　　(B.2)

③　$\displaystyle\int_1^\infty -\sqrt{\pi}\frac{\sqrt{zt}}{\sqrt{\bar{\gamma}_x}}e^{-\frac{zt}{\bar{\gamma}_x}}\mathrm{erf}\left(\frac{\sqrt{zt}}{\sqrt{\bar{\gamma}_x}}\right)\frac{e^{-\frac{t-1}{\bar{\gamma}_y}}}{\bar{\gamma}_y}e^{-\frac{t-1}{\bar{\gamma}_y}}dt,$　　(B.3)

④　$\displaystyle\int_1^\infty \sqrt{\pi}\frac{\sqrt{zt}}{\sqrt{\bar{\gamma}_x}}e^{-\frac{zt}{\bar{\gamma}_x}}\mathrm{erf}\left(\frac{\sqrt{zt}}{\sqrt{\bar{\gamma}_x}}\right)\frac{e^{-\frac{t-1}{\bar{\gamma}_y}}}{\sqrt{\bar{\gamma}_y}}\frac{\sqrt{t-1}\sqrt{\pi}}{\bar{\gamma}_y}dt,$　　(B.4)

⑤　$\displaystyle\int_1^\infty -\sqrt{\pi}\frac{\sqrt{zt}}{\sqrt{\bar{\gamma}_x}}e^{-\frac{zt}{\bar{\gamma}_x}}\mathrm{erf}\left(\frac{\sqrt{zt}}{\sqrt{\bar{\gamma}_x}}\right)\frac{e^{-\frac{t-1}{\bar{\gamma}_y}}}{\sqrt{\bar{\gamma}_y}}\frac{\sqrt{t-1}\sqrt{\pi}}{\bar{\gamma}_y}\mathrm{erf}\left(\frac{\sqrt{t-1}}{\sqrt{\bar{\gamma}_y}}\right)dt,$　　(B.5)

⑥　$\displaystyle\int_1^\infty -e^{-\frac{2zt}{\bar{\gamma}_x}}\frac{e^{-\frac{t-1}{\bar{\gamma}_y}}}{2\sqrt{\bar{\gamma}_y(t-1)}}\sqrt{\pi}dt,$　　(B.6)

⑦　$\displaystyle\int_1^\infty e^{-\frac{2zt}{\bar{\gamma}_x}}\frac{e^{-\frac{t-1}{\bar{\gamma}_y}}}{2\sqrt{\bar{\gamma}_y(t-1)}}\sqrt{\pi}\,\mathrm{erf}\left(\frac{\sqrt{t-1}}{\sqrt{\bar{\gamma}_y}}\right)dt,$　　(B.7)

⑧　$\displaystyle\int_1^\infty -e^{-\frac{2zt}{\bar{\gamma}_x}}\frac{e^{-\frac{t-1}{\bar{\gamma}_y}}}{\bar{\gamma}_y}e^{-\frac{t-1}{\bar{\gamma}_y}}dt,$　　(B.8)

⑨　$\displaystyle\int_1^\infty e^{-\frac{2zt}{\bar{\gamma}_x}}\frac{e^{-\frac{t-1}{\bar{\gamma}_y}}}{\sqrt{\bar{\gamma}_y}}\frac{\sqrt{t-1}\sqrt{\pi}}{\bar{\gamma}_y}dt,$　　(B.9)

⑩　$\displaystyle\int_1^\infty -e^{-\frac{2zt}{\bar{\gamma}_x}}\frac{e^{-\frac{t-1}{\bar{\gamma}_y}}}{\sqrt{\bar{\gamma}_y}}\frac{\sqrt{t-1}\sqrt{\pi}}{\bar{\gamma}_y}\mathrm{erf}\left(\frac{\sqrt{t-1}}{\sqrt{\bar{\gamma}_y}}\right)dt,$　　(B.10)

⑪　$\displaystyle\int_1^\infty \frac{e^{-\frac{t-1}{\bar{\gamma}_y}}}{2\sqrt{\bar{\gamma}_y(t-1)}}\sqrt{\pi}dt,$　　(B.11)

⑫　$\displaystyle\int_1^\infty -\frac{e^{-\frac{t-1}{\bar{\gamma}_y}}}{2\sqrt{\bar{\gamma}_y(t-1)}}\sqrt{\pi}\,\mathrm{erf}\left(\frac{\sqrt{t-1}}{\sqrt{\bar{\gamma}_y}}\right)dt,$　　(B.12)

⑬　$\displaystyle\int_1^\infty \frac{e^{-\frac{t-1}{\bar{\gamma}_y}}}{\bar{\gamma}_y}e^{-\frac{t-1}{\bar{\gamma}_y}}dt,$　　(B.13)

⑭　$\displaystyle\int_1^\infty -\frac{e^{-\frac{t-1}{\bar{\gamma}_y}}}{\sqrt{\bar{\gamma}_y}}\frac{\sqrt{t-1}\sqrt{\pi}}{\bar{\gamma}_y}dt,$　　(B.14)

⑮　$\displaystyle\int_1^\infty \frac{e^{-\frac{t-1}{\bar{\gamma}_y}}}{\sqrt{\bar{\gamma}_y}}\frac{\sqrt{t-1}\sqrt{\pi}}{\bar{\gamma}_y}\mathrm{erf}\left(\frac{\sqrt{t-1}}{\sqrt{\bar{\gamma}_y}}\right)dt.$　　(B.15)

The results obtained were:

$$a_z = 1 + \frac{\bar{\gamma}_x}{z\bar{\gamma}_y}, b_z = \frac{z}{\bar{\gamma}_x}, c_z = \frac{\bar{\gamma}_x}{z\bar{\gamma}_y}, k_i = \frac{(-1)^i}{i!(2i+1)}, \tag{B.16}$$

$$① = -\sqrt{\pi}\Gamma\left(\frac{1}{2}\right) e^{\frac{1}{\gamma_y}} \sum_{n=0}^{\infty} k_n \, a_z^{-\frac{n+\frac{5}{2}}{2}} \, b_z^{\frac{n+\frac{1}{2}}{2}} \, c_z^{\frac{1}{2}} \, e^{\frac{-a_z b_z}{2}} \, W_{\frac{n+3}{2}, \frac{-n-\frac{3}{2}}{2}}\left(a_z b_z\right), \tag{B.17}$$

$$② = 2 \cdot e^{\frac{1}{\gamma_y}} \sum_{n=0}^{\infty} \sum_{m=0}^{\infty} k_n \, k_m \, a_z^{-\frac{n+m+3}{2}} \, b_z^{\frac{n+m+1}{2}} \, c_z^{m+1} \, \Gamma(m+1) \, e^{\frac{-a_z b_z}{2}} W_{\frac{n-m+1}{2}, \frac{-n-m-2}{2}}\left(a_z b_z\right), \tag{B.18}$$

$$③ = -2 \, e^{-b_z} \sum_{n=0}^{\infty} \sum_{m=0}^{n+1} \frac{k_n \, (n+1)! \, b_z^m \, c_z}{m! \, (1+2c_z)^{n-m+2}}, \tag{B.19}$$

$$④ = 2 \, \sqrt{\pi} \, \Gamma\left(\frac{3}{2}\right) e^{\frac{1}{\gamma_y}} \sum_{n=0}^{\infty} k_n \, a_z^{-\frac{n+\frac{7}{2}}{2}} \, b_z^{\frac{n+\frac{3}{2}}{2}} \, c_z^{\frac{3}{2}} \, e^{\frac{-a_z b_z}{2}} \, W_{\frac{n+\frac{1}{2}}{2}, \frac{-n-\frac{5}{2}}{2}}\left(a_z b_z\right), \tag{B.20}$$

$$⑤ = -4e^{\frac{1}{\gamma_y}} \sum_{n=0}^{\infty} \sum_{m=0}^{\infty} k_n \, k_m \, a_z^{-\frac{n+m+4}{2}} \, b_z^{\frac{n+m+2}{2}} \, c_z^{m+2} \, \Gamma(m+2) \, e^{\frac{-a_z b_z}{2}} W_{\frac{n-m}{2}, \frac{-n-m-3}{2}}\left(a_z b_z\right), \tag{B.21}$$

$$⑥ = -\frac{\frac{\pi}{2}e^{-2b_z}}{\sqrt{1+\frac{2}{c_z}}}, \tag{B.22}$$

$$⑦ = \frac{e^{-2b_z}\left(\pi - 2\tan^{-1}\left(\sqrt{1+\frac{2}{c_z}}\right)\right)}{2\sqrt{1+\frac{2}{c_z}}}, \tag{B.23}$$

$$⑧ = -\frac{e^{-2b_z}}{2(1+\frac{1}{c_z})}, \tag{B.24}$$

$$⑨ = \frac{\pi e^{-2b_z}}{2(1+\frac{2}{c_z})^{\frac{3}{2}}}, \tag{B.25}$$

$$⑩ = -e^{-2b_z}\left(\frac{\pi}{2(1+\frac{2}{c_z})^{\frac{3}{2}}} - \frac{\tan^{-1}\left(\sqrt{1+\frac{2}{c_z}}\right)}{(1+\frac{2}{c_z})^{\frac{3}{2}}} + \frac{1}{2(1+\frac{2}{c_z})(2+\frac{2}{c_z})}\right), \tag{B.26}$$

$$⑪ = \frac{\pi}{2}, \tag{B.27}$$

$$⑫ = -\frac{\pi}{4}, \tag{B.28}$$

$$⑬ = \frac{1}{2}, \tag{B.29}$$

$$⑭ = -\frac{\pi}{2}, \tag{B.30}$$

$$⑮ = \frac{\pi}{4} + \frac{1}{2}. \tag{B.31}$$

For calculation of integrals ①-⑤, the following expressions were useful:

$$\text{erf}(x) = \frac{2}{\sqrt{\pi}} \sum_{n=0}^{\infty} \frac{(-1)^n x^{2n+1}}{n!(2n+1)}, \tag{B.32}$$

$$\int_u^{\infty} x^n e^{-\mu x} dx = e^{-u\mu} \sum_{k=0}^{n} \frac{n!}{k!} \frac{u^k}{\mu^{n-k+1}}, \tag{B.33}$$

$$\int_u^{\infty} x^{\nu-1}(x-u)^{\mu-1} e^{-\beta x} dx = \beta^{-\frac{\mu+\nu}{2}} u^{\frac{\mu+\nu-2}{2}} \Gamma(\mu) e^{\frac{-\beta u}{2}} W_{\frac{\nu-\mu}{2}, \frac{1-\mu-\nu}{2}}(\beta u), \tag{B.34}$$

where W is the Whittaker function.

For calculation of integrals ⑥-⑩ and ⑪-⑮, the following expressions were useful:

$$\int_0^{\infty} \frac{e^{-qx}}{\sqrt{x}} dx = \sqrt{\frac{\pi}{q}}, \tag{B.35}$$

$$\int_0^{\infty} \frac{1}{\sqrt{x}} \text{erfc}(\sqrt{x}) e^{-\beta x} dx = \frac{2\tan^{-1}(\sqrt{\beta})}{\sqrt{\pi\beta}}, \tag{B.36}$$

$$\int_0^{\infty} \sqrt{x} \, \text{erfc}(\sqrt{x}) e^{-\beta x} dx = \frac{1}{\sqrt{\pi}} \left(\frac{\tan^{-1}(\sqrt{\beta})}{\beta^{\frac{3}{2}}} - \frac{1}{\beta(1+\beta)} \right), \tag{B.37}$$

$$\int_0^{\infty} x^{n-\frac{1}{2}} e^{-\mu x} dx = \sqrt{\pi} 2^{-n} \mu^{-n-\frac{1}{2}} (2n-1)!!, \tag{B.38}$$

where (2n-1)!! denotes the double factorial, which is equal to $\frac{(2n)!}{2^n n!}$. The final expression is the sum of the integrals ①-⑮.